STREAMS

Smart Technologies for eneRgy Efficient Active cooling in Advanced Microelectronic Systems

H2020-ICT-2015-688564

STREAMS

Smart Technologies for eneRgy Efficient Active cooling in advanced Microelectronic Systems

Start date of the project: 01/01/2016
Duration: 42 months

D2.7

Versatile microfluidic actuation proof-of-concept demonstrated

WP	2	Versatile microfluidic actuation
Task	2.6	Versatile microfluidic actuation proof-of-concept

Dissemination Level[1]	PU
Nature[2]	D

Due Delivery Date	M34
Actual Delivery Date	17/07/2019

Lead beneficiary	UdL
Contributing beneficiaries	LN2, UdL, CEA, HSG, UFR-IMTEK, ST

Author	Proofreader
J. Barrau	Luc Fréchette

[1] Dissemination level: **PU** = Public, **PP** = Restricted to other programme participants (including the Commission services), **RE** = Restricted to a group specified by the consortium (including the JU), **CO** = Confidential, only for members of the consortium (including the Commission services).

[2] Nature of the deliverable: **R** = Report, **D** = Demonstrator, **O** = Other.

Document version	Date	Author	Comments[3]
v1	08/07/2019	J. Barrau (UdL)	Creation
v2	16/07/2019	L. Fréchette (LN2)	Modification
v3	17/07/2019	J. Barrau (UdL)	Final version for evaluation

[3] Creation, modification, final version for evaluation, revised version following evaluation, final.

Content

1. INTRODUCTION

The STREAMS project aims to improve the energy efficiency of microchannel cooling by reducing the pressure losses by 25%, while keeping the operating temperature and its uniformity within the appropriate ranges.

The present document aims to demonstrate these performances through the experimental assessment of a series of indicators, previously presented to the project reviewers and summarized in Table 1 Two state-of-the-art (SoA) approaches are also shown in comparison.

The solution tested in this Deliverable corresponds to the integration of the microfluidic solutions developed and verified in the previous tasks of this Work Package. This document will expose the experimental Proof of Concept results that lead to the experimental validation of these performances indicators.

Table 1. STREAMS objectives vs State of the Art for the cooling functionality.

Devices characteristics		STREAMS objective	STREAMS numerical assessment	SoA 1 Conventional Microchannels (*)	SoA 2 IBM [1]
Cooling technology		Self adaptive cooling device	Self adaptive cooling device or tailored Microchannel cooling device	Microchannels	Advanced Microchannels
Pressure drop		25% reduction	Max 0,03 bar	-	0,3 bar
Thermal Resistance		Equal	$1,7.10^{-5}$ Km^2/W	-	2.10^{-5} Km^2/W
Hydraulic Pumping Power (HPP)	Absolute	50% reduction	5% of Microchannel HPP	8 mW	-
	Relative	$HPP/P_{chip} < 0,05$ %	$HPP/P_{chip} = 0,02$ %	-	$HPP/P_{chip} = 0,17$ %

(*) Assessed numericaly in the STREAMS boundary conditions (See D2.1)

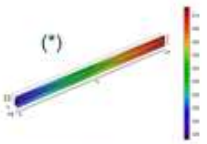

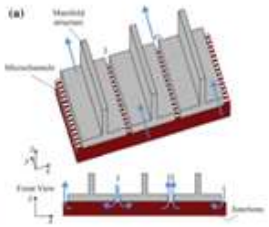

[1] Sharma, C. S. *et al.* (2015). Energy efficient hotspot-targeted embedded liquid cooling of electronics. Applied Energy, 138, 414–422

[1]

2. METHODOLOGY

The experimental characterization of the WP2 Proof of Concept was led by UdL, with the device microfabrication and packaging led by LN2. This work involved the following collaborations:

- HSG in a first stage, for the black box integration which incorporates the pump and mass flow control units.

- UdL and LN2. Along the WP2 activities, a straight collaboration and a weekly communication have been implemented between LN2 and UdL. Furthermore, two members of UdL team have been working at LN2, for different STREAMS tasks, but mainly in relation to Task 2.6. These coordination actions ensured good communication between the involved teams.
- STREAMS consortium. A Joint measurement day (19/06/2019), before M42 General Assembly in Lleida, allowed to implement the last measurements (Figure 1). Also a Demo session has been planned in the M42 General Assembly (20/06/2019).

Joint measurement day Demo session at M42 GA

Figure 1. STREAMS consortium for PoC tasks and Demo session(GA).

2.1. Test bench

The schematic design of the experimental setup used for this study is shown in Figure 2.

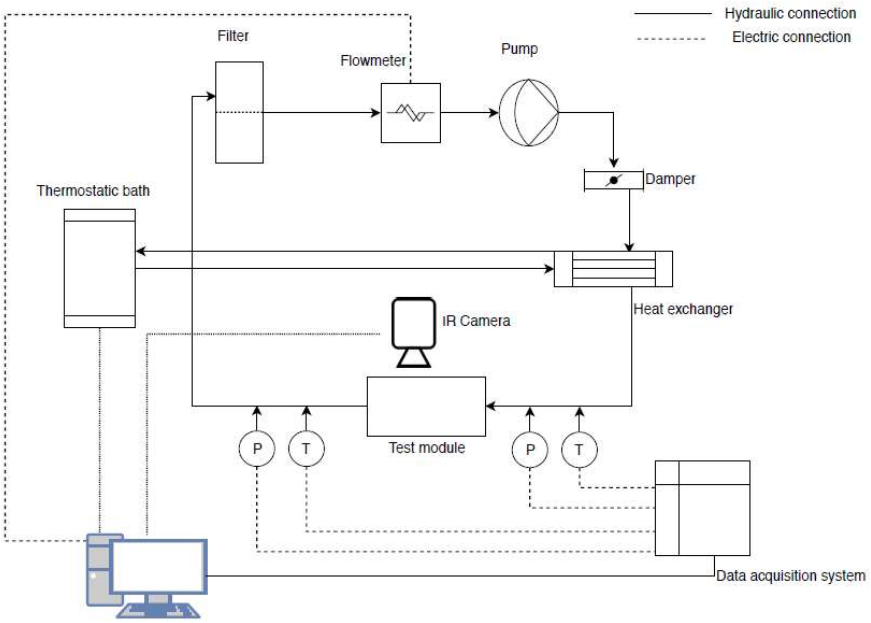

Figure 2. Fluidic test module setup.

The microfluidic experimental setup is based on two separated hydraulic circuits. In the first one, the water is stored in a thermostatic bath (PolyScience PD07R20-20-A12E) which is thermally connected to the heat exchanger responsible for heating or cooling the water of the second circuit. This second circuit is composed of a 1 µm filter (Shelco MPX) connected to a flowmeter (Bronkhorst mini cori-flow M15) and then to a micro-diaphragm liquid pump (KNF NF5). A diaphragm pulsation damper (KNF FPD06/1.06-Z), placed after the pump, is responsible for flow stabilization before it enters the heat exchanger. Then, the test module is hydraulically connected to the heat exchanger and finally the water returns to the filter. Type T thermocouples are used to measure inlet and outlet water temperatures and two pressure sensors measure the pressure drop across the device.

Finally, an infrared camera (Flir A655sc) is used for measuring the surface temperatures of the test module. A data acquisition system (Agilent 34970A) collects the information from the test bench and send them to the computer, where Labview software is used to process it (Figure 3).

Figure 3. Fluidic test module in UdL Lab.

Heat load

For the assessment of the Self-Adaptive fins impact on the thermo-hydraulic performance of the cooling device (Chapter 3.1), the test module is heated with an external Kapton flexible heater (Birk BK3561) that can give up to 20 W/cm^2 and is electrically connected with a programmable power source (PSI9200-04T), which can be controlled with LabVIEW software.

For the tests with fixed coolant flow rates (Chapter 3.2.1), one peripheral and the central integrated heaters are powered for each sample assessed (Figure 4). Heater B for MC and MC6T_Qvalve and heater C for MC6T. In each case the power density given is 80 W/cm^2 for the CH heater and 60 W/cm^2 for the PH heater (13,47 W in total).

For the other tests (Tailored flow rates, chapter 3.2.2), two peripheral and central integrated heaters, both in common Thermal Test Chips (TTCs), are powered for each sample assessed.

The inlet temperature is maintained constant through the thermostatic bath.

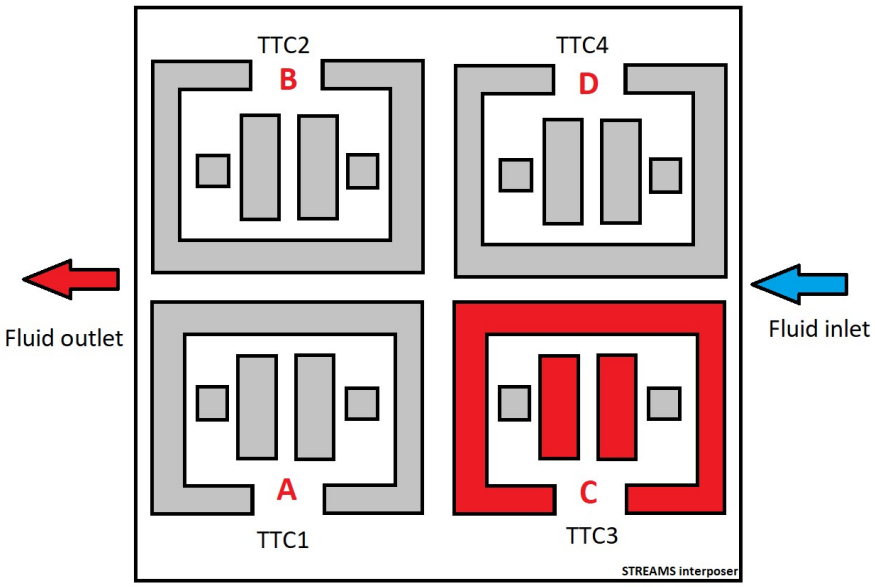

Figure 4. Schematic of the heaters with CH and PH heaters opened in one TTC.

The temperature measurements of the chip surface are carried out through the RTDs and the IR camera. The emissivity of the surface has been calibrated, leading to difference of temperatures measurements between both systems lower than 5 %.

2.2. Fabrication

2.2.1. Design configuration

The microfluidic chip consists of an assembly of 3 layers. Layer 1, made of a silicon wafer, contains cavities, straight or tailored microchannels on the bottom side. On the top side, it contains heaters made of nickel. The heat sources are fabricated as metallic serpentines for Ohmic heating, which also serves as RTDs for temperature measurement. In layer 2, made of silicon, the self-adaptive microvalves and fins were fabricated on the top side. Layer 3 is made of polyimide film (Kapton) for the fluidic inlet/outlet (Figure 5). This triple stack is then mounted on a plastic (ABS) flow distributor which in integrated in the packaging.

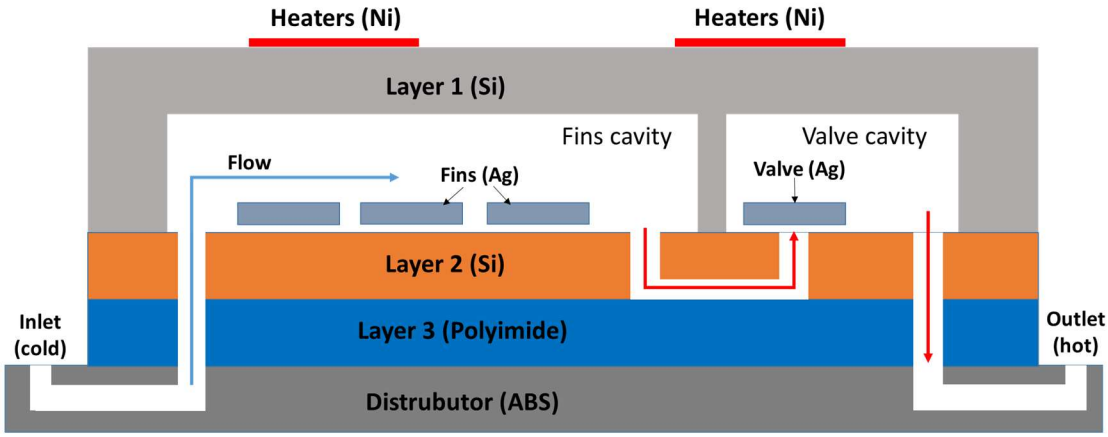

Figure 5. Schematic cross-section view of the fluidic device.

2.2.2. Process flow

Fabrication of layer 1:

Layer 1 is fabricated through clean room processes on a double side polished 4" Si wafer of 330 or 525 µm thick (Figure 6). The process flow of layer 1 having microheaters (top side) and the cavities (on the back side) is shown below (

Table 2).

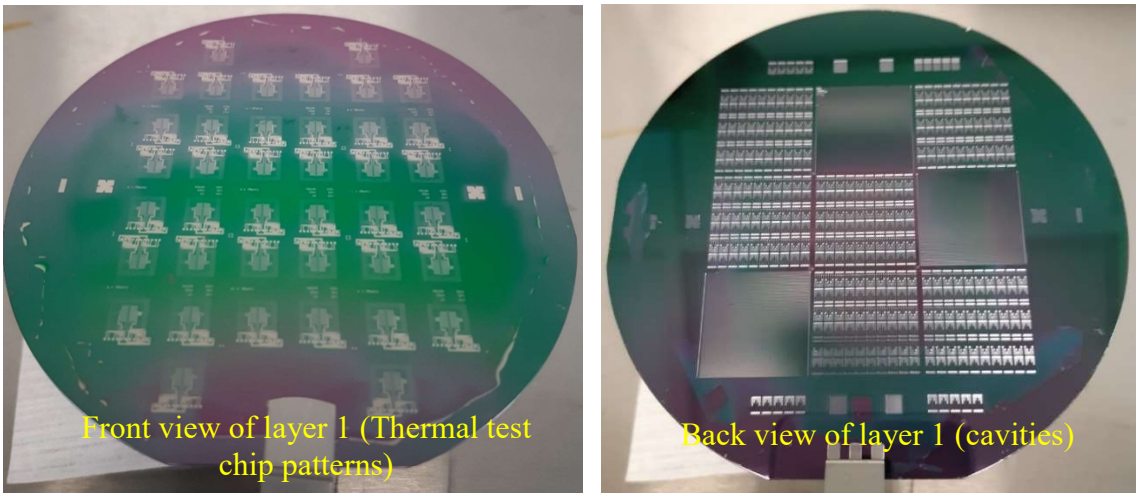

Figure 6. Front view and back side of layer 1.

Table 2. Microfabrication process flow of layer 1.

1	Wafer Cleaning	Opticlear, Acetone, IPA, water, N_2 drying + RCA (SC-2)	
2	SiO_2 deposition	Thermal Oxide growth: 1 µm Cleaning: SC-1	
3	Metallization	50 nm Cr and 200 nm Au	
4	Photoresist deposition	*Adhesion promoter (MCC Primer)*: drying 180 °C @ 5 min; softbake 110°C @ 1 min *Photoresist (AZ 1518)* Coat: 500rpm for 5s and then 4000rpm for 60s Softbake: 110 °C for 1 min	
5	Photolithography	Exposure time 6s (alignment mask, heaters mask) Develop for 45 s with MF319 (non-diluted)	
6	Electroplating (heaters)	Heaters: Electrolyte: Elevate Nickel 40 Anode: High purity Ni electrode Current: 29.9 mA (10 mA/cm²) with agitation with 4.4 min for each	

		microheater for 0.9 µm thickness	
7	Photoresist stripping	With acetone	
8	Metal removing	Gold etch 8148 (Ni compatible) for 45s Chrome etch CR7S10 for 60s	
9	SiO_2 Sputtering	Device: 2, 5, 8 (3 µm thick passivation) Device: 1B. 2B, 3B (300 nm)	
10	Photoresist deposition	Hydration: 110°C for 5 min MCC primer; softbake 110°C for 1 min Photoresist (AZ 1518); softbake 110°C for 1 min	
11	Photolithography	SiO_2 Passivation Mask Exposure time 10 sec Develop for 1-2 min with MF 319 (non-diluted)	
12	Electric pad exposition (Oxide wet etch)	Buffered Oxide Etch (BOE) Etching time: 3 min 30 s	
13	PR stripping	Acetone, IPA, H_2O	
14	SiO_2 etch	AOE of 1 µm SiO_2 Cell cavities/microchannels	

15	Si etch	*DRIE of 80/400 µm of Si* *Cell cavities/microchannels*	
16	SiO_2 wet etch	HF etch of 1 µm of SiO_2 on the bottom side	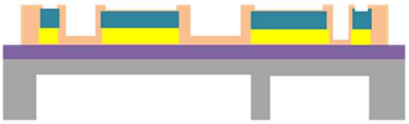
17	Metallization	20 nm Cr, 50 nm Pt and 500 nm Au Prior to eutectic bonding	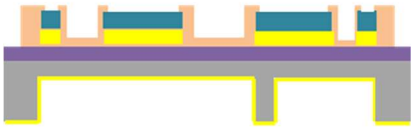

Fabrication of layer 2:

Layer 2 (microvalves and fins) is fabricated through clean room processes on a 4" Si wafer of 330 µm thick. Two versions of layer 2 are fabricated as shown in Figure 7. The process flow of layer 2 is shown in Table 3.

Table 3. Microfabrication process flow of layer 2.

1	Wafer Cleaning	Opticlear, Acetone, IPA, water, N_2 drying + RCA (SC-2)	
2	SiO_2 deposition	PECVD: 2 µm Cleaning: SC-1	
3	SiO_2 etch	AOE of 700 nm SiO_2 Eccentricities	
4	SiO_2 etch	AOE of 1300 nm SiO_2 *Anchors*	
5	Photolithography + Metallization + liftoff	9 µm Ag deposition (evaporation) and liftoff Valves/Fins	
6	SiO_2 etch	AOE of 2 µm SiO_2 Nested mask	

		Elbow	
7	SiO_2 etch	AOE of 2 µm SiO_2 Nested mask Inlet/outlet/valve hole	
8	Si etch	DRIE of 200 µm Si Nested mask Inlet/outlet/valve hole	
9	Si etch	DRIE of 100 µm Si Nested mask Inlet/outlet/valve hole/elbow	
10	SiO_2 wet etch	HF etch of 2 µm of SiO_2	

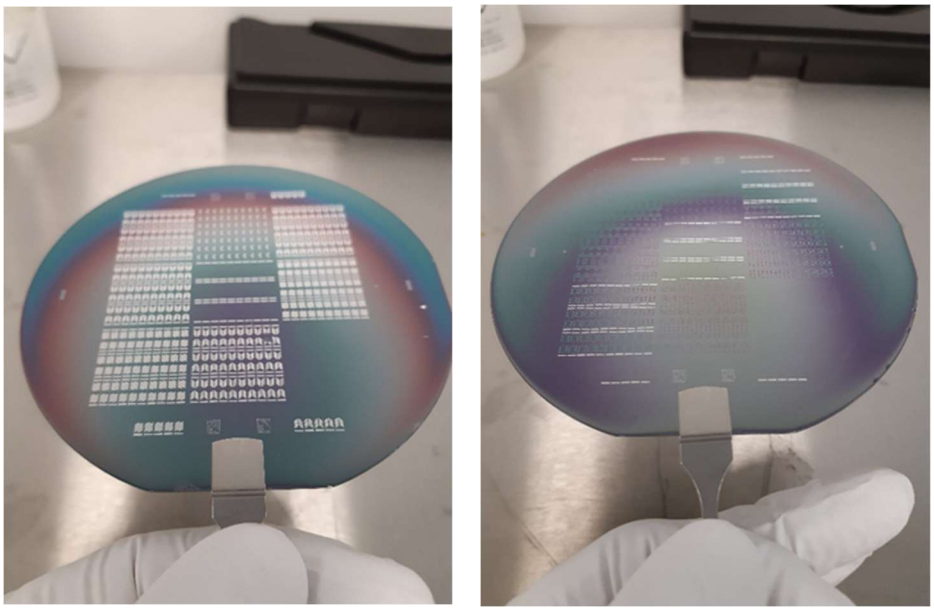

(a) (b)

Figure 7. Front view of layer 2. (a) Version 1; (b) Version 2.

Modification in the fabrication of layer 3 (inlet/outlet) and wafer-to-wafer bonding:

Layer 3 (fluidic inlet/outlet) is fabricated using polyimide film (Kapton HN of thickness 125 µm, Figure 8). The process flow of the layer 3 is shown below (Table 4):

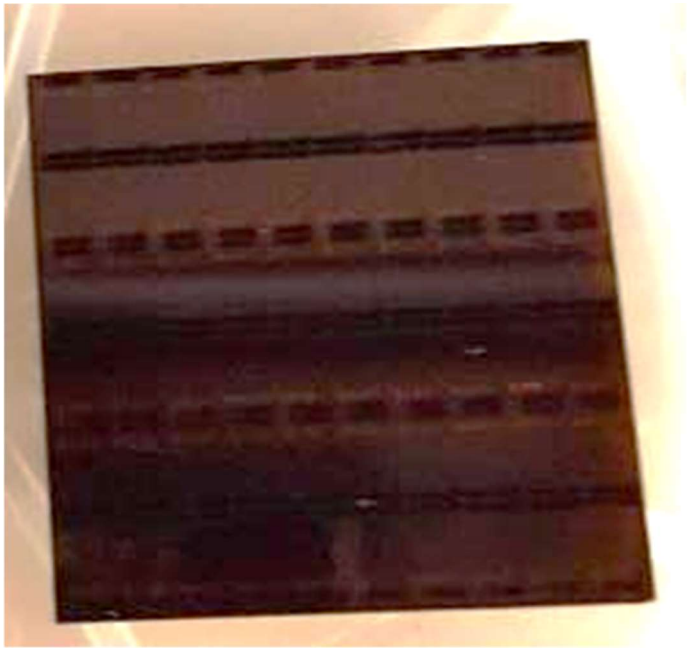

Figure 8. Microfluidic device having Kapton as layer 3 for fluidic inlet/outlet.

Table 4. Microfabrication process flow for layer 3.

1	Plasma cleaning of Kapton Power 100 W for 7 mins
2	Photoresist Spinning PERMINEX 1000 3000 RPM; 60 s; softbake at 95 °C for 5 min
3	UV expose of Kapton using Aligner OAI 200 for 50 s
4	Lamination of exposed Kapton on stack of layer 1-2 at 70 ° C
5	Bonding and laser etching for trenches

2.2.3. Assembly

Layers 1, 2 and 3 are stacked to form the fluidic devices (Table 5)

Table 5. Process flow of the entire assembly.

1	Bonding	Si/Au Eutectic bonding Layer 1 to layer 2 380 degC, 30 min	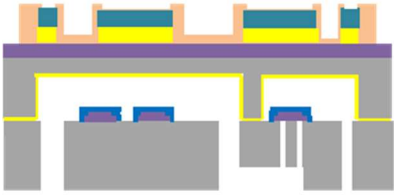
2	SiO_2 wet etch	Buffered Oxide Etch (BOE) Valves/Fins releasing Etch time: 10 h	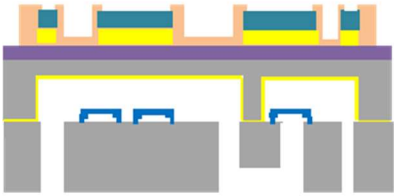
3	Bonding	Adhesive bonding with Kapton film Stack 1-2 to layer 3 Temperature: 150 °C; 60 s; applied force: 1000 N; 0.5 MPa; Curing time: 1 hour in-situ in the bonding tool	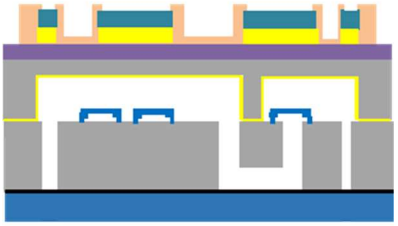
4	Laser etching	Etching holes through Kapton film LPKF Protolaser U3; Source: YAG pumped by diodes (355 nm); Size of the opened trenches: 100 µm	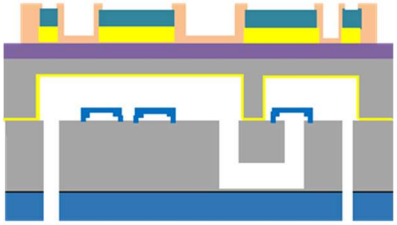

2.2.4. Packaging

Fluidic connection from below the chip

In this version of the chip, the fluidic supply and collection is done from below the chip. Figure 9 shows that the connection ports are distributed in rows under the entire surface of the chip. For supply and collection, interdigitated channels are used, as shown in Figure 10. The channels are built inside a distribution layer in ABS, printed in 3D. To seal between the channels on the underside, an epoxy adhesive is spread on the walls separating the channels and the periphery of the chip as shown in Figure 11.

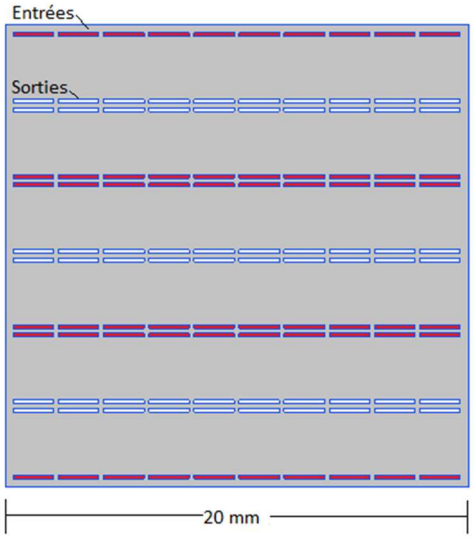

Figure 9. Backside view of the fluidic chip showing the inlet/outlet configuration.

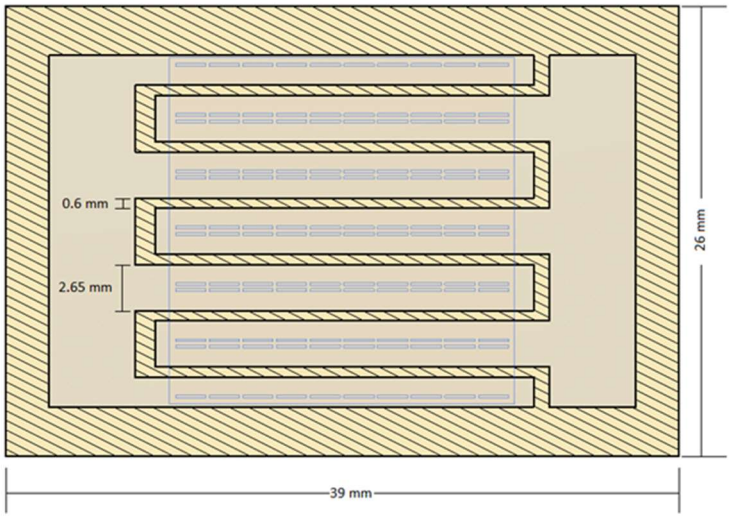

Figure 10. Cross-section view of the distributor, overlaid with the inlets and outlets (gray).

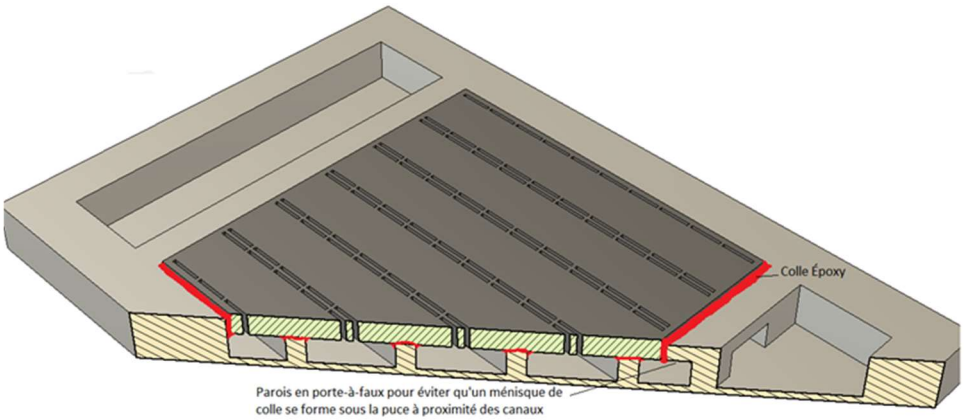

Figure 11. Cross-section view of the distributor showing the sealing with the epoxy (red).

2.2.5. Design of the distributor

The design addresses two main needs: the distribution and collection of fluid, as well as the tightness between the channels and the outside.

The fluid distribution is done through open interdigital channels. The size of the walls between the channels, here set at 0.6 mm, was chosen to ensure that the 3D printing process produces the walls in two passes of material width. The upper surface above the walls also keeps more glue and limits the risk of unglued areas. With the width of the channels being fixed by design, only the depth of the channels can be modified to minimize the losses of load if required. The walls of the channels are also kept straight to maximize the distance between the inlets/outlets of the chip and the menisci glue and to prevent small openings soak the adhesive by capillarity.

To avoid imbibing the glue, the seal to the outside must be made by the sides of the chip because of the proximity of the channels with the sides of the chip. For this purpose, the walls around the chip are left cantilevered to control the formation of meniscus glue under the chip.

Fluidic connections to the distributor are provided by integrating a 3D printed barded connector, which allows the press-fit insertion onto inlet/outlet tubes from the test set-up. In addition, a 3D printed ABS frame surrounds the device onto which a cover (not shown) can be mounted for protection during shipping and handling.

2.2.6. Summary of the fabricated devices

Table 6 summarizes the successfully fabricated devices and Figure 12 shows the complete packaged devices.

Table 6. Summary of the fabricated samples.

	Device No.	Type	Heaters	SiO_2 passivation
VERSION. 1 (channels depth=400 µm)	N379F-2	MF cells without valves (cell arrays)	Fabricated on layer 1	3 um
	N379F-5	MF cells with valves	Fabricated on layer 1	3 um
	N379F-8	Microchannels	Fabricated on layer 1	3 um

VERSION. 2 (channels depth=80 µm)	N379-1B	MF cells with valves-fins	Separate chip glued on layer 1 (Ag epoxy)	300 nm
	N379-3B	MF cells with valves	Separate chip glued on layer 1 (Ag epoxy)	300 nm

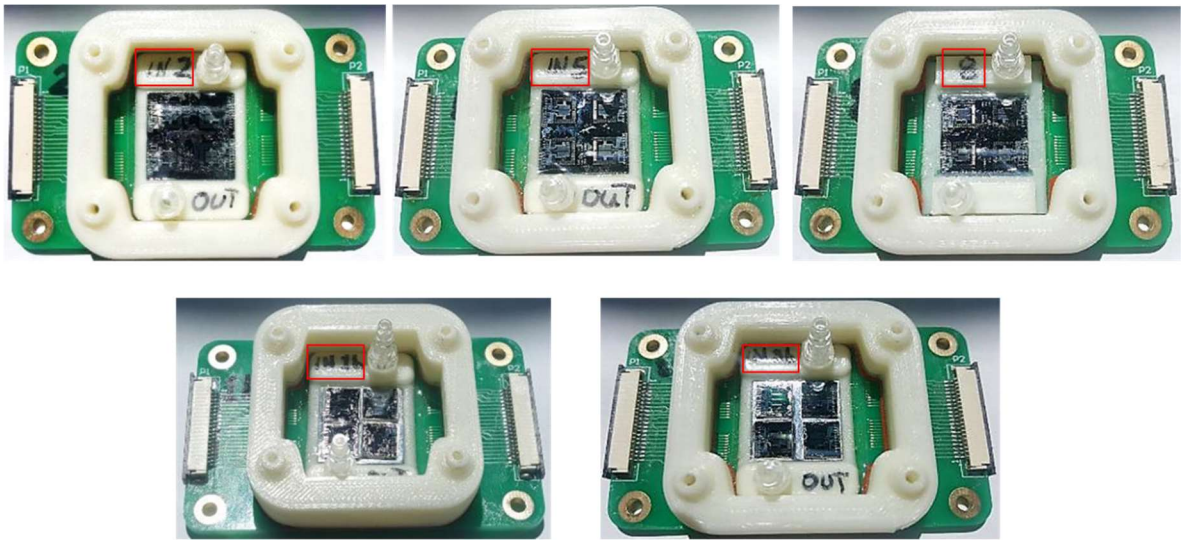

Figure 12. Image of the complete packaged WP2 Microfluidic PoC devices.

2.2.7. Wire bonding of heaters (fluidic devices) to interposer PCB

The devices under test were wire bonded to the interposer PCB. The type of bond chosen was a wedge bond, with the wire bonds made out of a 25 µm aluminum wire. Because of their length, the ampacity of the bonds was limited to 200 mA. The bonds were therefore doubled on the common output terminal where all currents from the heaters are collected.

To allow an infrared optical access to the surface of the devices, no encapsulation was used on its top surface. However, due to their very long length, and the need to protect them in shipping, a flexible encapsulation (Polydimethylsiloxanes, or PDMS) was used with an adhesion primer on the base of the wires. The ABS frame therefore also served to define the zone covered by PDMS around the chip.

2.2.8. Electrical characterization of the heaters

The required heat power to apply on the fluidic device was calculated after measuring the resistance of the different heaters (Table 7). Most heater were successfully characterized, but some were found to be damaged or in open circuit (red).

Table 7. Electrical characterization of the heaters.

Device	P1 (DC resistance in Ohm relative to pin 10 or 20) +-1%																	
	Outer Heater 1		Heater 1a		Center Heater 1		Heater 1b		Com 1	Outer Heater 2		Heater 2a		Center Heater 2		Heater 2b		Com 2
name	1	2	3	4	5	6	7	8	9	11	12	13	14	15	16	17	18	19
1b	1013	1020	623	595	945	957	590	544	3	923	929	608	583	868	880	532	491	3
2	2340	2330	1428	1355	ouv.	ouv.	1138	1041	3	ouv.	ouv.	ouv.	1350	2040	2070	ouv.	1000	2
3b	882	887	558	534	ouv.	837	508	471	3	ouv.	ouv.	ouv.	ouv.	ouv.	ouv.	ouv.	ouv.	3
5	1898	1911	1045	988	1754	1778	949	869	3	1795	1806	1065	1011	2710	1694	ouv.	ouv.	2
8	1676	1682	ouv.	ouv.	ouv.	ouv.	ouv.	ouv.	3	1852	1861	784	748	1641	1664	ouv.	ouv.	2
Device	P2 (DC resistance in Ohm relative to pin 10 or 20) +-1%																	
	Outer Heater 1		Heater 1a		Center Heater 1		Heater 1b		Com 1	Outer Heater 2		Heater 2a		Center Heater 2		Heater 2b		Com 2
Name	1	2	3	4	5	6	7	8	9	11	12	13	14	15	16	17	18	19
1b	846	851	492	471	775	786	502	467	3	893	ouv.	528	503	837	849	506	469	3
2	2280	2290	1037	992	1996	2050	ouv.	ouv.	3	2180	2190	1023	980	1954	1974	1211	1128	3
3b	929	935	545	524	868	880	591	553	2	894	900	498	477	845	855	581	544	2
5	1932	1941	ouv.	ouv.	1749	1771	1070	997	2	2060	2060	1007	966	1835	1860	1112	1036	2
8	1820	1830	992	939	1661	1683	864	790	3	1644	1653	ouv.	ouv.	1514	ouv.	793	727	2

Legend		
	####	Regular
	ouv.	Heater is accessible from an other pin
	ouv.	Heater is either missing or both traces are broken

2.2.9. Characterization of the valves

Different tests were done with an optical profilometer to determine the resulting geometry and the reaction to a temperature rise of the Ag microvalves. Since the bonding of layer 1 with layer 2 was done before releasing the valves, they were characterized from the backside (through the

inlet/outlet hole). The Ag microvalve showed both clean surface and a complete release of the sacrificial layer in most of the cases. The structure is placed on a hot plate under the optical profilometer and the hot plate temperature is measured and controlled with a type K thermocouple and a PID. Results showed that the microvalves effectively bend upward with the temperature rise, confirming that the double clamped beam and its thermal expansion principle can be reproduced with success. The microvalve also presented an elastic behavior, essential for the cell durability (Table 8, Table 9, Table 10).

The topology is first investigated at room temperature. The valves showed excellent geometric properties, that are based on the following criteria: the microvalve surface flatness and the height between the Si and the top of the valve. In addition to the optical profilometer, visual inspection with an optical microscope showed that the holes below the valves are opened up to the valve.

Two temperature points are taken to make sure that the microvalves work properly: the first one at room temperature and the second one is exposed on a hot plate at 80 °C. The actual temperature of the microvalve is unknown due to the thermal interface resistance between the samples and the hot plate. The summary of those tests is presented in tables 8, 9 and 10 for the devices N-379F-5, N379-1B and N379-3B respectively. When heated, the microvalve centers raised. It can be seen that most of the microvalves showed a significant opening with temperature.

Table 8. Deflection of the valves for device N379F-5.

	Valve 1	Valve 2	Valve 3	Valve 4	Valve 5	Valve 6	Valve 7	Valve 8	Valve 9	Valve 10
Row 1	9.2 µm	Flat	14	10	OK	17	OK	5	Flat	OK
Row 2	16	15	OK	OK	OK	OK	OK	OK	OK	OK
Row 3	16	16	18	OK	OK	OK	Flat	OK	Flat	OK
Row 4	15	Flat	OK	15	OK	10	OK	7	13	OK
Row 5	15	11	18	OK	OK	OK	OK	OK	OK	OK
Row 6	13	17	14	12	OK	12	OK	9	Ok	13

Table 9. Deflection of the valves for device N379-1B.

Valve 1	Valve 2	Valve 3	Valve 4	Valve 5	Valve 6	Valve 7	Valve 8	Valve 9	Valve 10

Row 1	N.V.	N.V.	15 um	15	N.V.	N.V.	N.V.	N.V.	15	N.V.	**80 °C**
Row 1	N.V.	N.V.	16	17	N.V.	N.V.	N.V.	N.V.	17	N.V.	**150 °C /2mins**
Row 1	N.V.	N.V.	6	3	N.V.	N.V.	N.V.	N.V.	3	N.V.	**R.T (20 °C)**

Table 10. Deflection of the valves for device N379-3B.

	Valve 1	Valve 2	Valve 3	Valve 4	Valve 5	Valve 6	Valve 7	Valve 8	Valve 9	Valve 10
Row 1	Flat	18 um	OK	OK	Flat	Flat	18	Flat	OK	Flat
Row 2	15	OK	OK	9	OK	Flat	OK	20	Flat	Flat
Row 3	Flat	15	OK	NO	OK	15	OK	OK	OK	11
Row 4	OK	OK	15	15	Flat	OK	Flat	15	Flat	OK
Row 5	18	OK	OK	Flat	Flat	17	OK	OK	15	Flat
Row 6	OK	Flat	Flat	OK	18	NO	NO	Flat	NO	Flat

Note:

N.V: valves are not verified/characterized

Values in µm: dz, experimentally measured

OK: the valves buckles perfectly (confirmed through fringes), but dz not measured

Flat: Buckling in opposite direction (this will be reversed with the flow pressure)

NO: Missing valves/broken

2.3. Tested geometries and references

Table 11 presents the list of tests planned for WP2 PoC demonstration. For each device, the boundary conditions to be applied, the reference sample to be compared with and the objectives of the associated tests are described. This extended list aims to cover the demonstration of the STREAMS objectives related to the cooling functionality but also to provide material for future publications.

Based on the set of devices successfully fabricated, part of the planned tests was possible, and will be described in detail in the following section. The consortium has focused its effort to produce the devices mandatory for the demonstration of the STREAMS objectives.

Table 11. Relation of planned cooling geometries and tests.

Priority	TEST ID	Date	Sample		Objective		to be compared with... (ID test / ID sample)	Heat load scenario	Flow rate
			ID	Description	Quantitative	Description			
1	T1_1		H400_MC6T	Array of µfluidic cells MC6T		base sample for comparison with T1_2		STREAMS scenario 3	Q cnt
1	T1_2		H400_MC6T_Qvalve	Array of µfluidic cells MC6T + Q valve	Ppump < 20%, Tuniformity	Impact of the valve inside MC6T cell (D2.2 POC). All heaters open	T1_1	STREAMS scenario 3	Constant - Qvalve
1	T1_3		H400_MC6T	Array of µfluidic cells MC6T		base sample for comparison with T1_4		STREAMS scenario 2	Constant
1	T1_4		H400_MC6T_Qvalve	Array of µfluidic cells MC6T + Q valve	Tunifomity	Impact of the valve inside MC6T cell when only central heater open	T1_3	STREAMS scenario 2	Constant - Qvalve
2	T2_1		H80_MCH	Long straigh MC, Hch=80		base sample for comparison with T2_2		STREAMS scenario 1	Constant
2	T2_2		H80_MCH_VaF	Mc with VaF, Hch=80	Nu/Nu0, f/f0, Tchip_av, TPF for different Re	Assess the impact of VaF inside a mch for different Re. Comparison with numerical values (D2.2 POC)	T2_1	STREAMS scenario 1	Constant
2	T2_3		H80_MCH	Long straigh MC, Hch=80		base sample for comparison with T2_4		STREAMS scenario 3	Constant
2	T2_4		H80_MCH_VaF	Mc with VaF, Hch=80	Nu/Nu0, f/f0, Tchip_av, TPF for different Re and transient heat load scenario	Assess the impact of VaF inside a mch for different Re and time dependent scenario	T2_3	STREAMS scenario 3	Constant
2	T2_5		H80_MCH	Long straigh MC, Hch=80		base sample for comparison with T2_6		STREAMS scenario 4	Constant
2	T2_6		H80_MCH_VaF	Mc with VaF, Hch=80	Nu/Nu0, f/f0, Tchip_av, TPF for different Re and transient heat load scenario	Assess the impact of VaF inside a mch for different Re and time dependent scenario	T2_5	STREAMS scenario 4	Constant
3	T3_1		H80_MC0	Array of µfluidic cells MC0 + Q valve		base sample for comparison with T3_2,3,4,5		STREAMS scenario 1	Constant-Qvalve
3	T3_2		H80_MC0_VaF2	Array of µfluidic cells MC0 + Q valve + VaF diagonal	Nus/Nu0, f/f0, TPf for different Re	Impact of VaFs inside a cell for different fin configuration and different Re. Objective: Find the best configuration	T3_1, T3_3	STREAMS scenario 1	Constant-Qvalve

3. Proof of Concept RESULTS

3.1. Impact of self-adaptive fins in a microchannel device (steady state)

The objective of this test is to experimentally assess the thermo-hydraulic performance that the self-adaptive fins perform inside a microchannel cooling device compared with plain microchannels. The test module used for validation of the numerical model is based on 7 plain microchannels of 1950 µm width, 19500 µm length and 80 µm height, with a wall thickness of 975 µm (Figure 13).

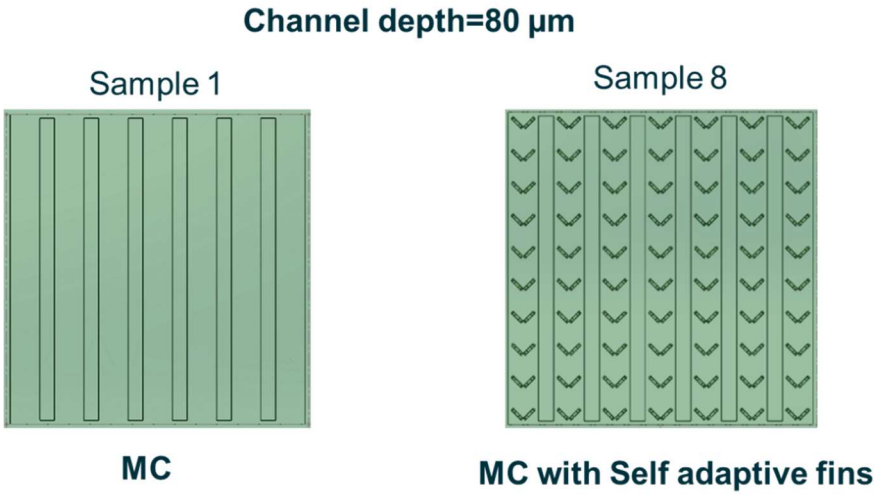

Figure 13. Variation of temperature under unsteady heat flux.

However, it is found that only two lateral microchannels have fins inside while in the rest of them, the traces of the anchors of the fins are seen but not the fins itself (Figure 14). This lack of the fins can be attributed to microfabrication defects or to an overpressure in which the fins were submitted in previous tests.

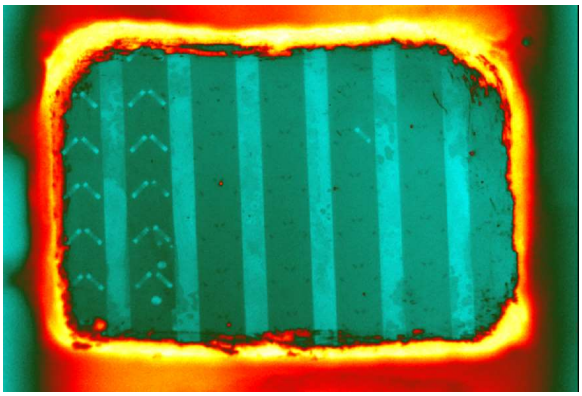

Figure 14. Infrared camera image of the Si microchannels with self-adaptive fins (seen through the Si wall).

In order to do an equal comparison, the two microchannels with self-adaptive fins are heated with an external flexible heater with a heating area of 0.64 x 0.64 cm^2 (Figure 15), that gives a heat flux of 7.5 W/cm^2 to the channels, while the other channels are sealed. Meanwhile, on the other sample, the 7 plain microchannels are heated with a bigger heater, that covers all the channels, and gives an equal heat flux.

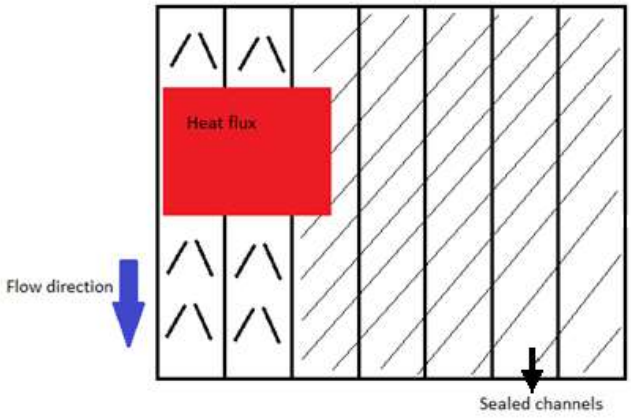

Figure 15. Schematic of the heating configuration applied on 2 microchannels with self-adaptive fins

Temperature uniformity along one microchannel is assessed when both devices are submitted to proportional non-uniform heat fluxes and two different flow rates, equivalent to Q = 5.5 ml/min per channel and Q = 7.5 ml/min per channel (Figure 16). It is seen that, for the same flow rate, microchannels with self-adaptive fins present a lower thermal gradient, what can be an indicative parameter of the performance of the fins.

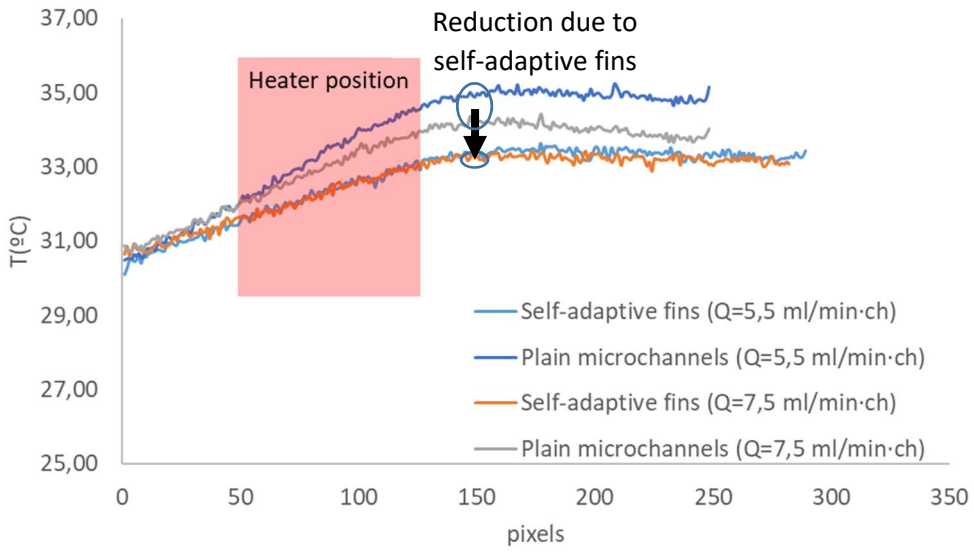

Figure 16. Non-uniform heating of (a) Self-adaptive fins: q'=3,07 W and (b) Plain microchannels: q'=10,75.

Visualization of the self-adaptive fin deformation through thermal IR camera

The deformation of the self-adaptive fins inside a microchannel has been observed through the thermal analysis of the infrared camera when the device is submitted to a uniform heat flux (Figure 17). In this case, when the temperature is assessed outside the position of the fins, a linear evolution of the temperature along the microchannel is seen (Figure 17a). Moreover, when the temperature is plotted along a line that goes through the anchors of the fins, we notice a clear dip in the measurement at the anchors, which follows the trend of the wall temperature (Figure 17b). This is to be expected since the anchors are in direct contact with the wall and should therefore follow the same temperature distribution. The measurement difference between the wall and the anchor (the dip itself) does not necessarily represent a difference in temperature, since the emissivities of the wall and beam are different. Finally, when the measurement is plotted along a line that crosses the middle of the fins, an interesting profile is obtained (Figure 17c). At the entrance of the channel, where the temperature is lower, the fins remain in flat position and so they remain at a temperature near that of the anchors because no water flows below them. However, as the temperature increases along the channel, the self-adaptive fins rise up, allowing the water to pass below them and cooling them. Then, what is seen through the IR camera is that the temperature at the position of the fin becomes more uniform with the surroundings and the temperature peaks gets much smaller because it is showing the water temperature. Although this is a qualitative assessment, it gives an idea of the self-adaptive behavior of the fins inside a microchannel.

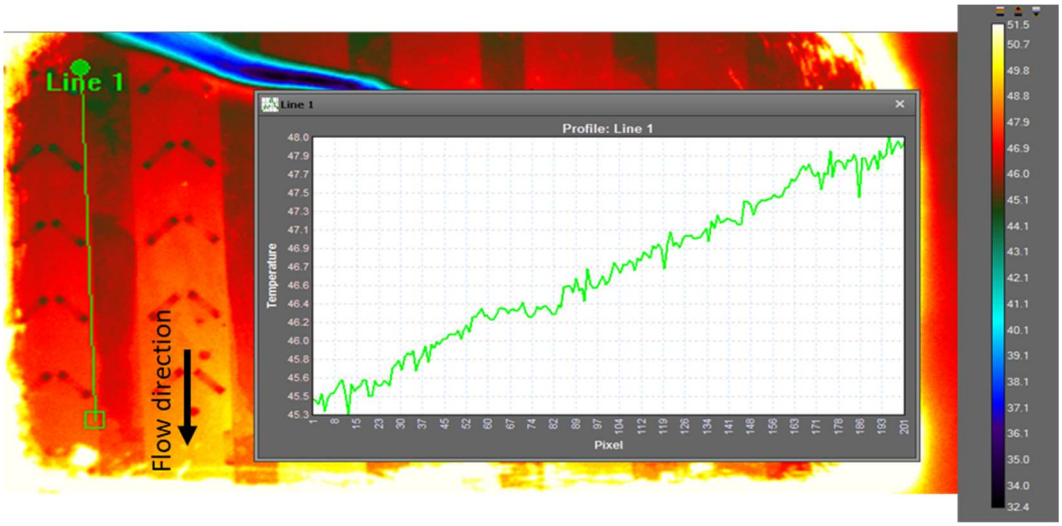

(a)

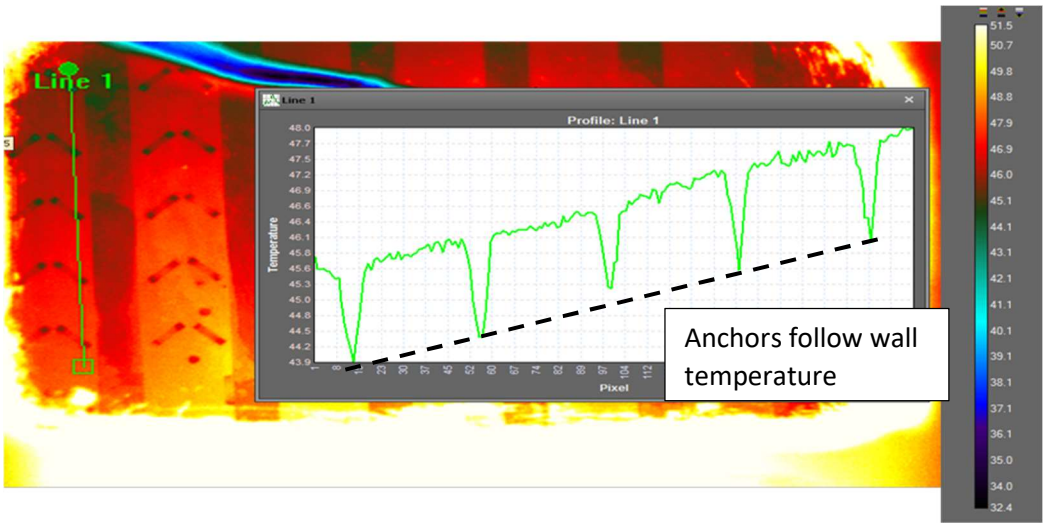

(b)

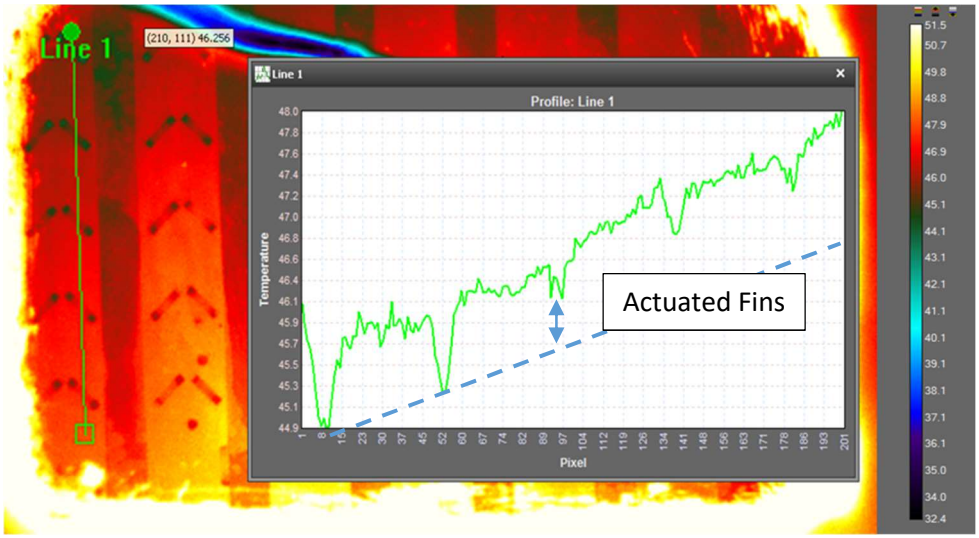

(c)

Figure 17. Temperature evolution along the microchannel for different positions of "Line 1": (a) Outside the self-adaptive fins, (b) Above the anchors and (c) Above the self-adaptive fins.

3.2. Performance of the microfluidic cell array with Self-Adaptive valves

The devices tested in this section correspond to the array of 60 microfluidic cells (with and without Self-Adaptive valves) and the reference microchannel device (Figure 18). The depth of the etched channels is 400 µm.

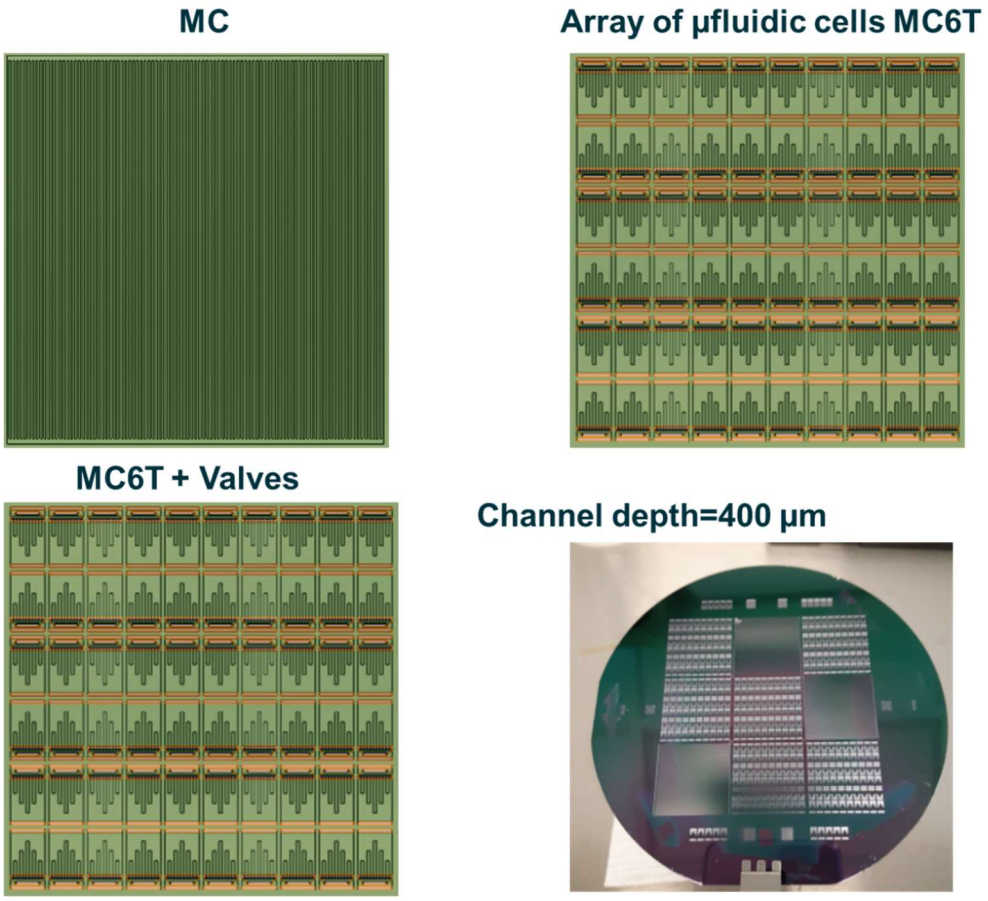

Figure 18. Geometries of the tested samples.

For the array of microfluidic cells, a distributor has been designed to feed, with a minimum pressure drop, coolant with a similar inlet temperature to each of the cells. The microchannel device is however fed from the edges of the chip, and has an adapted packaging.

3.2.1. Fixed flow rate - Assessment of steady state performance

Pressure drop

The pressure drop in the devices is evaluated at fixed flow rate, applying a reference heat load of 13,47 W. The pressure drop of the array of microfluidic cells (MC6T) presents a reduction of 81.5% with respect to the microchannel device (MC) at low flow rate (Q=16ml/min). This proportion is similar for higher flow rates (Figure 19).

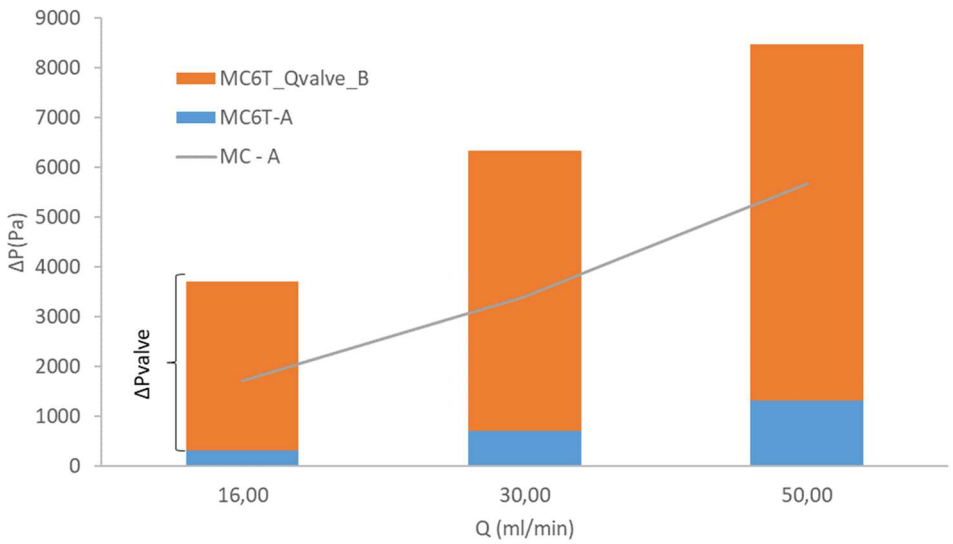

Figure 19. Pressure drop.

This result demonstrates that the STREAMS cooling scheme allow to reduce drastically one of the major drawback of microchannel cooling devices: large pressure drops. For constant flow rate, this implies a reduction in the hydraulic pumping power of MC6T with respect to MC, between 75 and 82% (Figure 20).

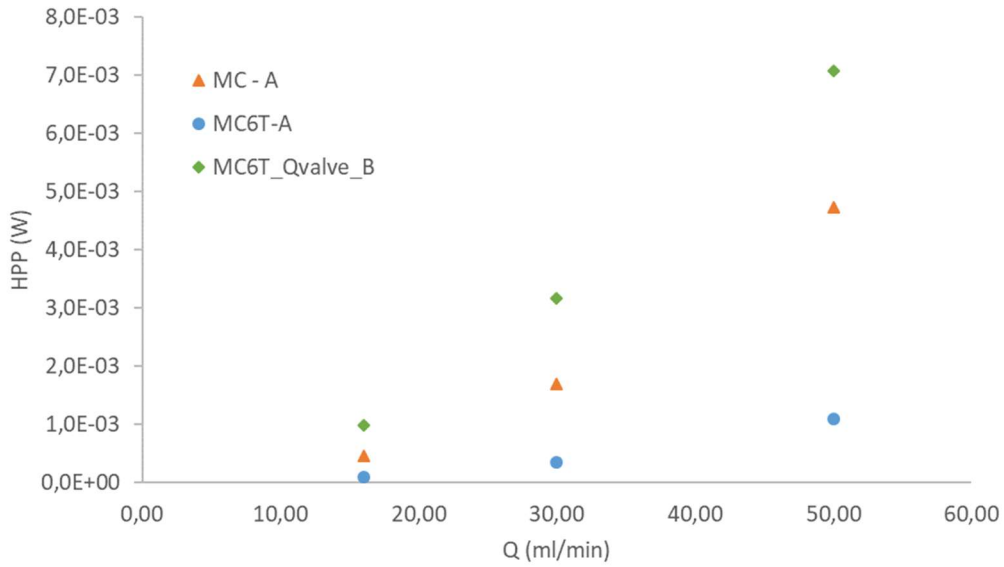

Figure 20. Hydraulic Pumping Power (HPP).

For the array of microfluidic cells with Self-Adaptive valves controlling the flow rate distribution (MC6T_Qvalve), the additional pressure drop generated by the valves (much higher than the pressure drop generated by the flow path within the microfluidic cell) implies that the pressure

drop is higher than for the other tested devices. This characteristic is mandatory to allow the temperature dependent Self-Adaptive valves to act as a passive control of the coolant distribution. Note that fixed flow rate is considered in this test and few self-adaptive valves are open due to small heat load. In real operating conditions (non-uniform and time-dependent Heat Load Scenarios (HLS)), this behavior does not cause a major impact on the Hydraulic Pumping Power (HPP), as the flow rate is reduced (related to the PID control of the total flow rate, see 3.2.2) until there's need of higher heat extraction capacity.

Thermal resistance

However, the total thermal resistance of the microchannel cooling device is lower (but in the same order of magnitude) than for the array of microfluidic cells (Figure 21).

This is due to the fact that the geometry of the array of microfluidic cells (MC6T) generates a flow rate, inside the tailored channels (Figure 22) that is 3.6 times lower than in any one of the microchannels. In addition, for MC6T, these tailored channels represent only 1/3 of the flow length in the microfluidic cells. Furthermore, the hydraulic diameter is higher in MC6T than in MC, so the Reynolds number inside the tailored channels is 5,8 times lower in the array of microfluidic cells than in microchannels.

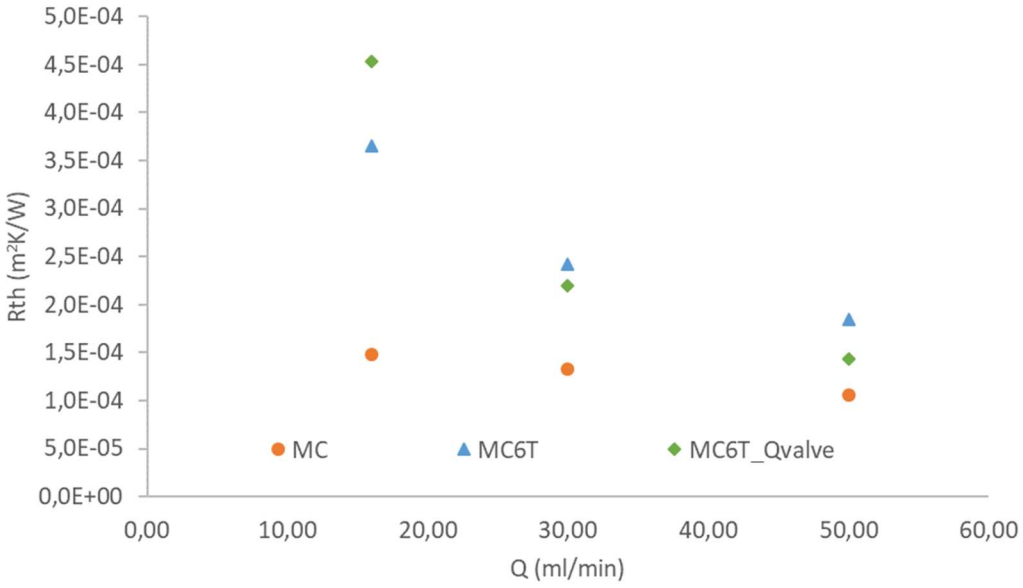

Figure 21.Thermal resistance coefficient.

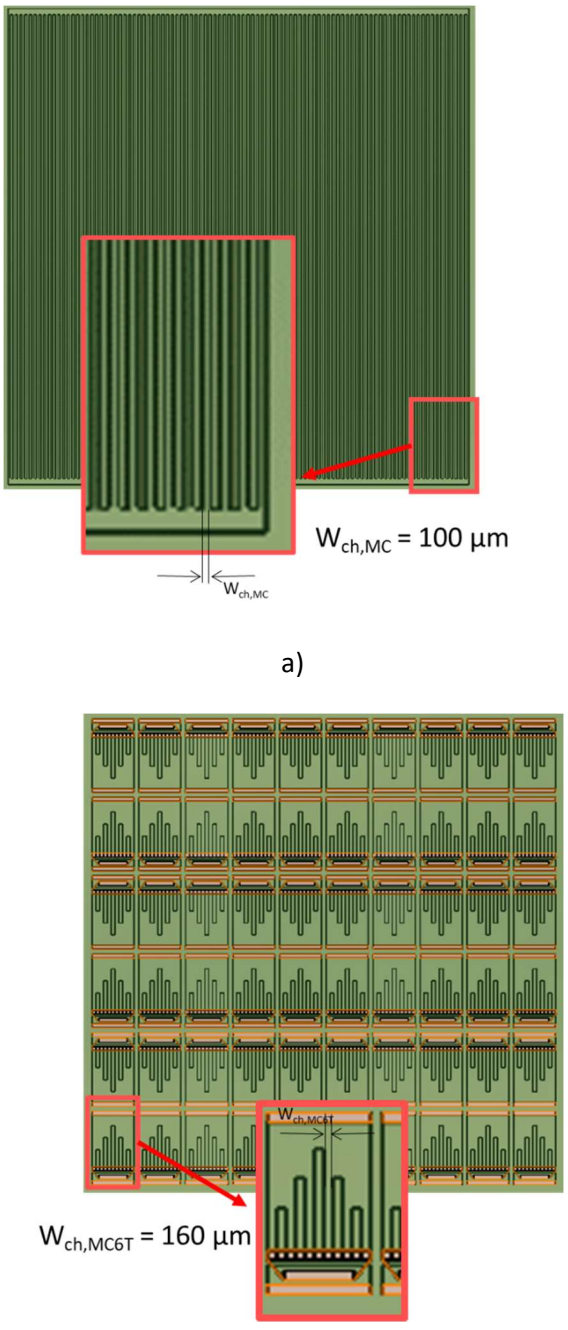

Figure 22. Detail of the channel geometries.

The difference of thermal resistance between the microchannel device and the array of microfluidic cells with Self-Adaptive valves decreases when the flow rate increases. This behavior, also observable for the maximum and average temperatures of the chip surface (Figure 23), indicates that, locally, the tailored distribution of coolant allows to feed more coolant flow rate where the heat extraction capacity needs to be augmented, leading to a decrease of the local thermal resistance for the microfluidic cells with the major heat flux.

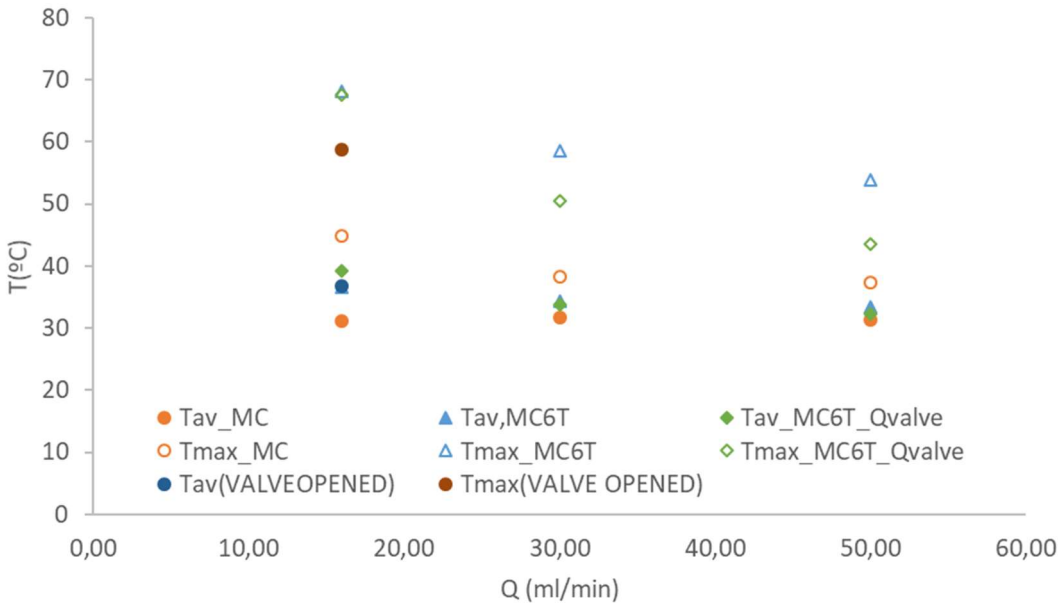

Figure 23.Variation of temperatures (T_{av} refers to the average surface temperature and T_{max} to the maximum surface temperature).

Temperature distribution

The temperature pattern of MC6T depends only on the heat flux distribution (Figure 24), as the geometry generates a uniform heat extraction capacity with a similar inlet temperature of the coolant for each microfluidic cell. This demonstrates a key feature of the cell array configuration.

For the array of microfluidic cells with self-adaptive valves (MC6T+Valve), the temperature distribution pattern corresponds to the geometry of the microfluidic cells. This result confirms the capacity of the STREAMS cooling solution to tailor the distribution of the heat extraction capacity for transient and non-uniform heat load scenarios. In conclusion, in the microfluidic cells array, local heat extraction is achieved and heat load time and space heterogeneity is managed adequately.

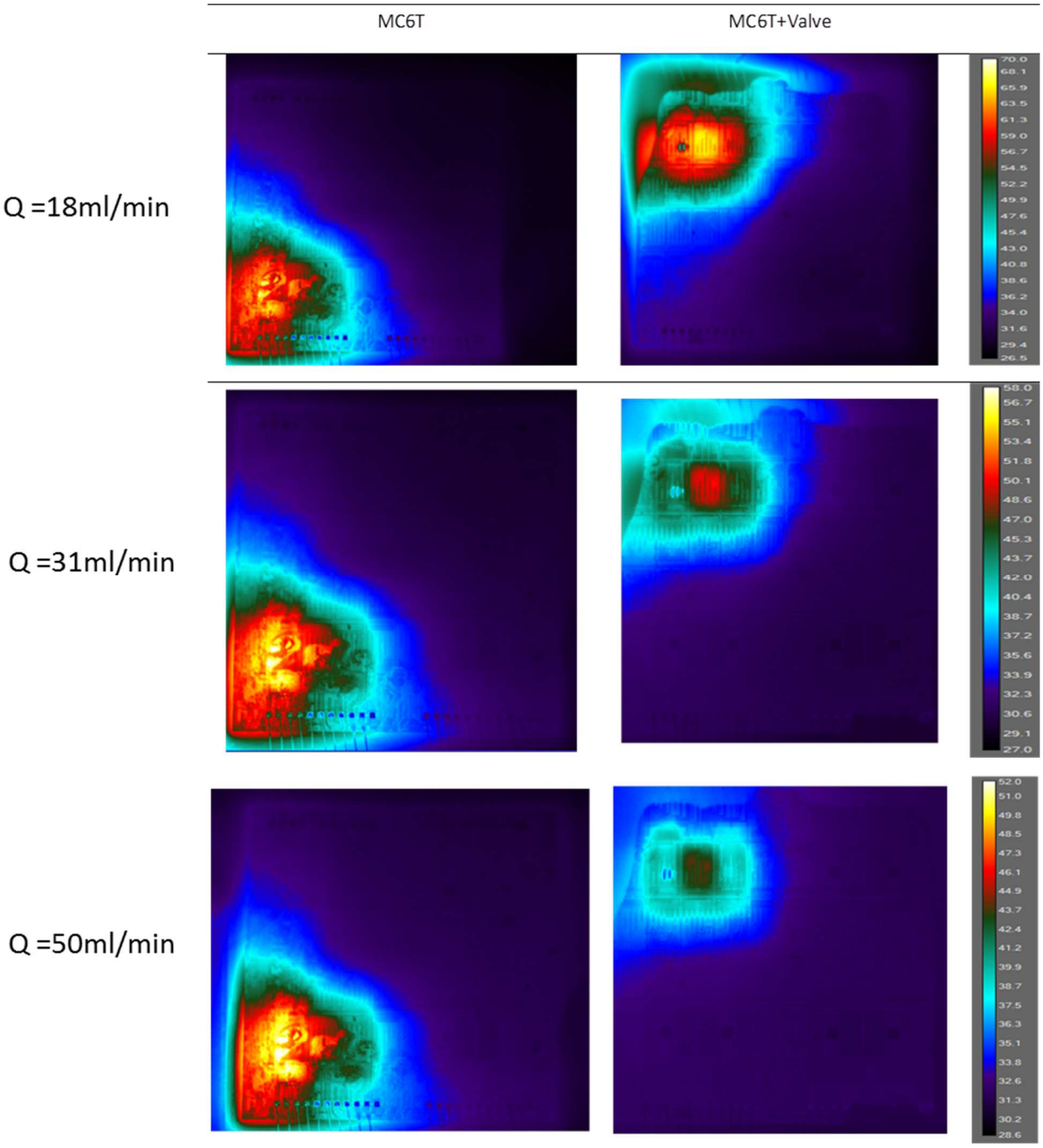

Figure 24.Temperature distribution for one Peripheral and one Central heater powered, for the microfluidic cell arrays. Note that the color scale differs for each flow rate.

On the contrary, for the microchannel device, we can observe in Figure 25 (Q = 12, 17, 31, 50 ml/min with a heater ON at the beginning of the flow path of the microchannel device), that the temperature distribution of this cooling scheme depends both on the heat flux distribution and on the geometry of the device.

Indeed, we can observe propagation of heat in the direction of the flow path due to the heated coolant transported along this direction.

Q=12ml/min	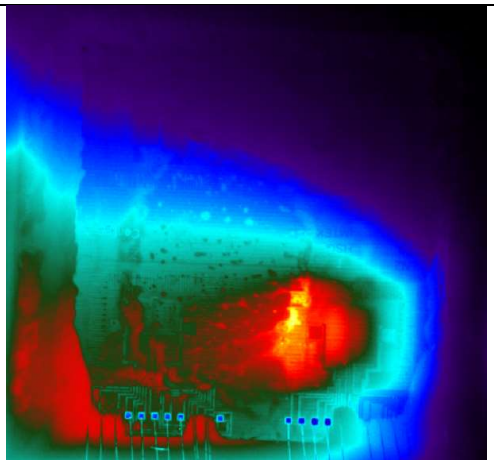	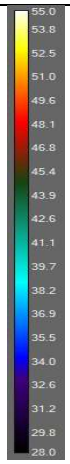
Q=17 ml/min	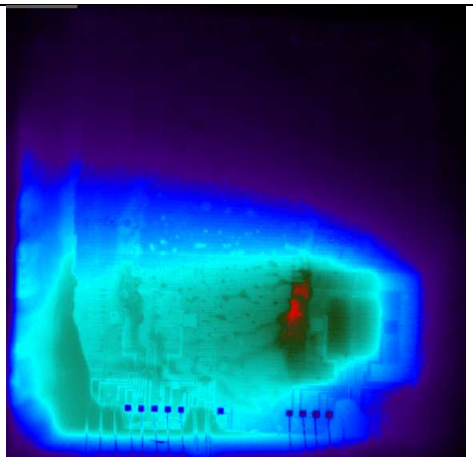	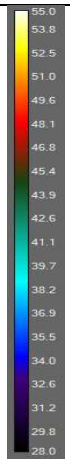
Q = 30 ml/min	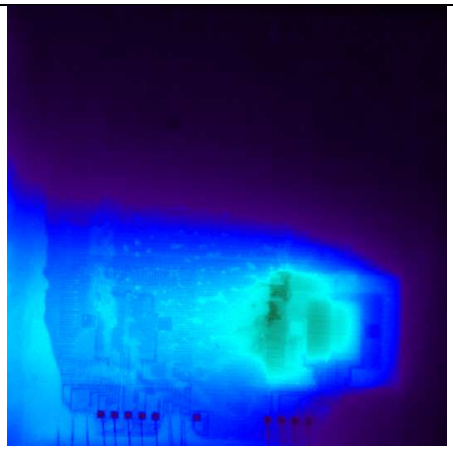	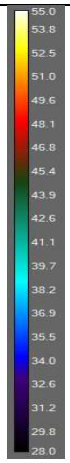

Q = 50 ml/min

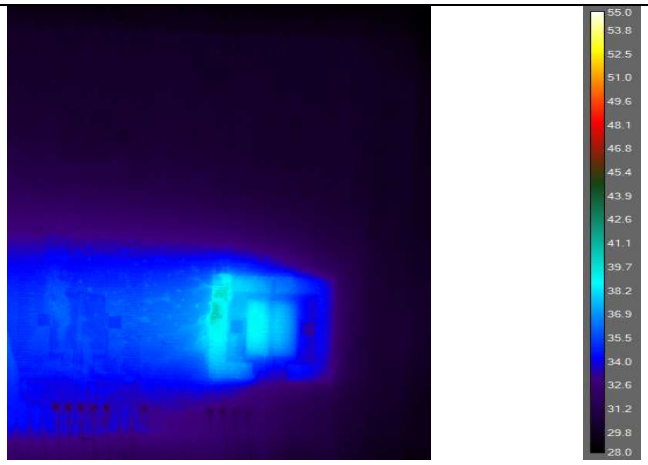

Figure 25. Temperature distribution in microchannels for several flow rates. Inlet of the microchannels is on the right of the picture and outlet on the left.

Validation of the impact of the Self-Adaptive valves on the thermo-hydraulic performance

For the array of microfluidic cells with self-adaptive valves (MC6T+Valve), the effect on temperature dependence of the flow rate distribution has been observed. For a given set of fixed boundary conditions (Inlet temperature; Flow rate; Heat flux), the opening and closing of the self-adaptive valves, leading to a passive control of the distribution of the heat extraction capacity, has been validated (Figure 26Figure 28).

For the first set of constant boundary conditions (Q=6.5 ml/min, q''_{CH} = 80W/cm^2, q''_{PH} = 60 W/cm^2), a video, which can be found at the project website: http://project-streams.eu/dissemination/, demonstrates more clearly this behavior, which is central for the STREAMS cooling validation. The following figures (Figure 26, Figure 27, Figure 28) give numerical insight of the behavior. Figure 26 shows the two basic characteristics of microfluidic cells regulated by self-adaptive valves: (1) the cooling flow rate is locally regulated attending to maximum temperature designed and (2) the local thermo-hydraulic response is almost instantaneous. The regulation is more stable (less oscillations) when the flow rate is increased and when the heat load decreases, and the magnitude of the temperature difference between the open/close positions of the valves behave in similar ways (Figure 29).

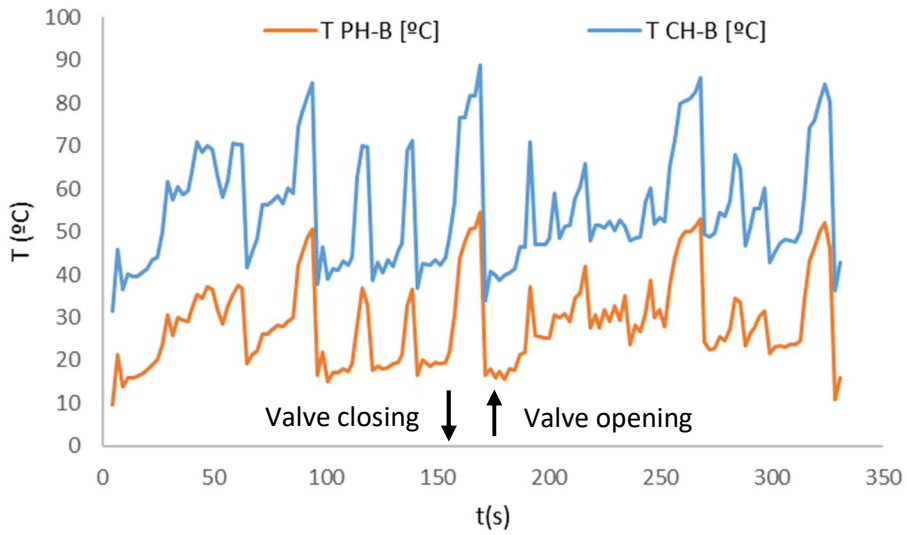

Figure 26. Maximum temperature variation over time at fixed boundary conditions (Q = 6.5 ml/min, q''_{CH} = 80 W/cm², q''_{PH} = 60 W/cm²).

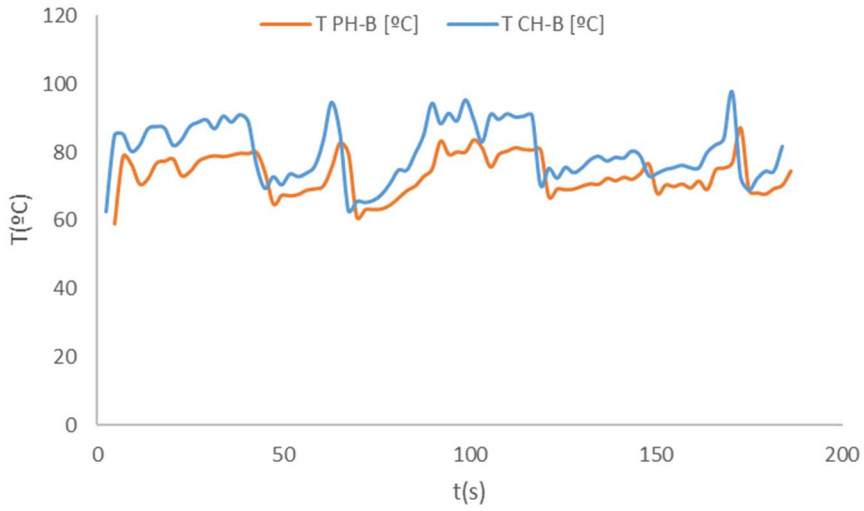

Figure 27. Maximum temperature variation over time at fixed boundary conditions (Q=16.6 ml/min, q''_{CH} = 80 W/cm², q''_{PH} = 60 W/cm²).

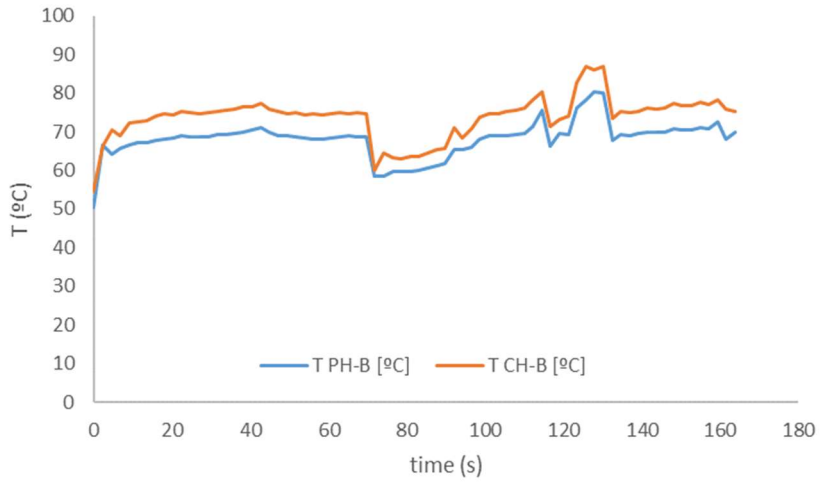

Figure 28. Maximum temperature variation over time at fixed boundary conditions (Q=16 ml/min, q''_{CH} = 64 W/cm², q''_{PH} = 48 W/cm²).

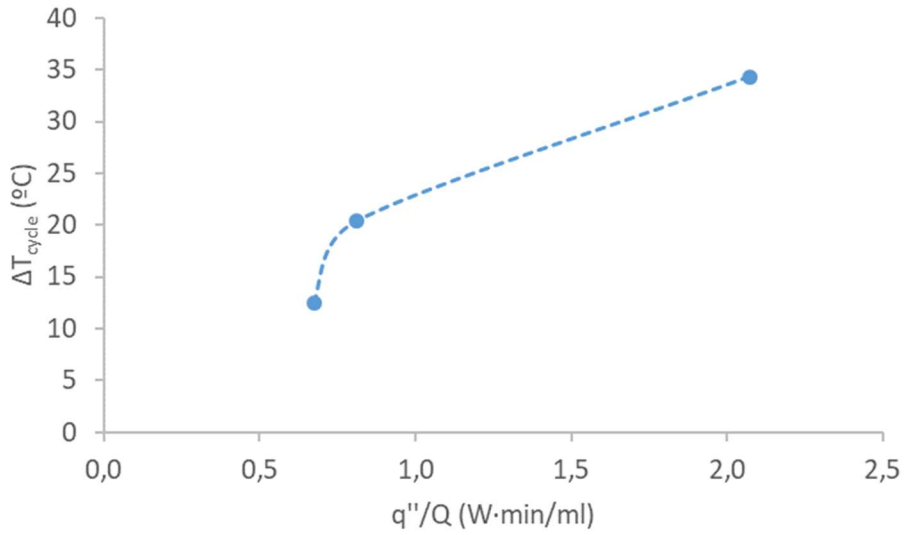

Figure 29. Average temperature variation by cycle as a function of the boundary conditions.

As expected, due the geometry of the cooling solutions, the global thermal resistance of the array of microfluidic cells is higher than for microchannels. **However, it has been demonstrated in this chapter that the minimum local thermal resistance is similar in both devices thanks to the capacity of the STREAMS solution to tailor the coolant distribution to the heat load distribution**.

3.2.2. *Variable flow rate - Time-dependent and non-uniform Heat Load Scenarios*

The novelty carried by the STREAMS cooling solution comes from its ability to tailor the distribution of heat extraction capacity to time-dependent and non-uniform Heat Load Scenarios, in order to both reduce the Hydraulic Pumping Power and the temperature non-uniformities across the chip. The objective of this chapter is to experimentally demonstrate this performance.

In this chapter, a transient and non-uniform (2/4 TTCs powered) heat load scenario is applied (Figure 30) while the flow rate is tailored, through an optimized PID control, to the maximum temperature of the chip surface.

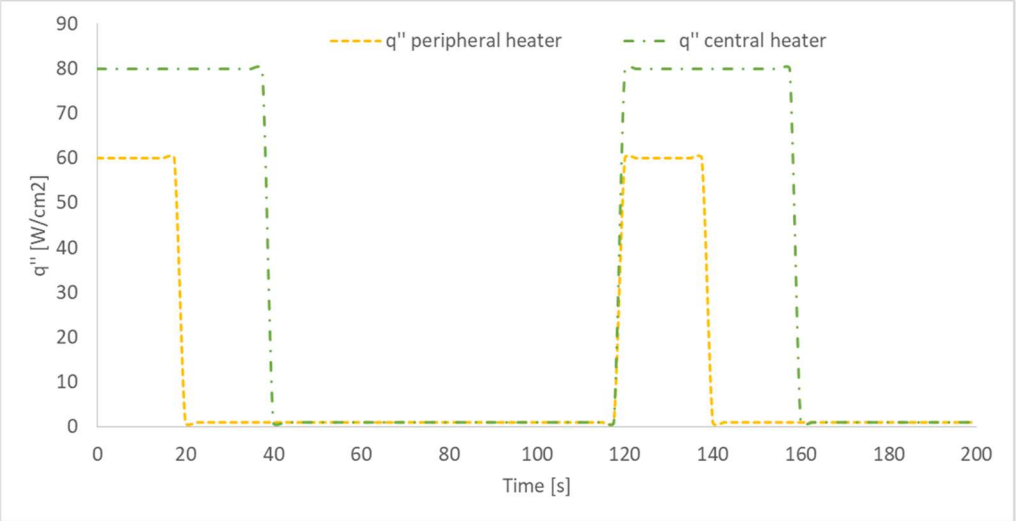

Figure 30. Transient heat load scenario.

Thermal resistance

The maximum temperature of the devices is similar in microchannels and the array of microfluidic cells with Self-Adaptive valves (Figure 31), demonstrating the capacity of the STREAMS cooling solution to achieve low local thermal resistances through the passive control of the coolant distribution (Figure 32). Meanwhile, the array of microfluidic cells without Self-Adaptive valves reach higher temperatures even with higher total flow rates.

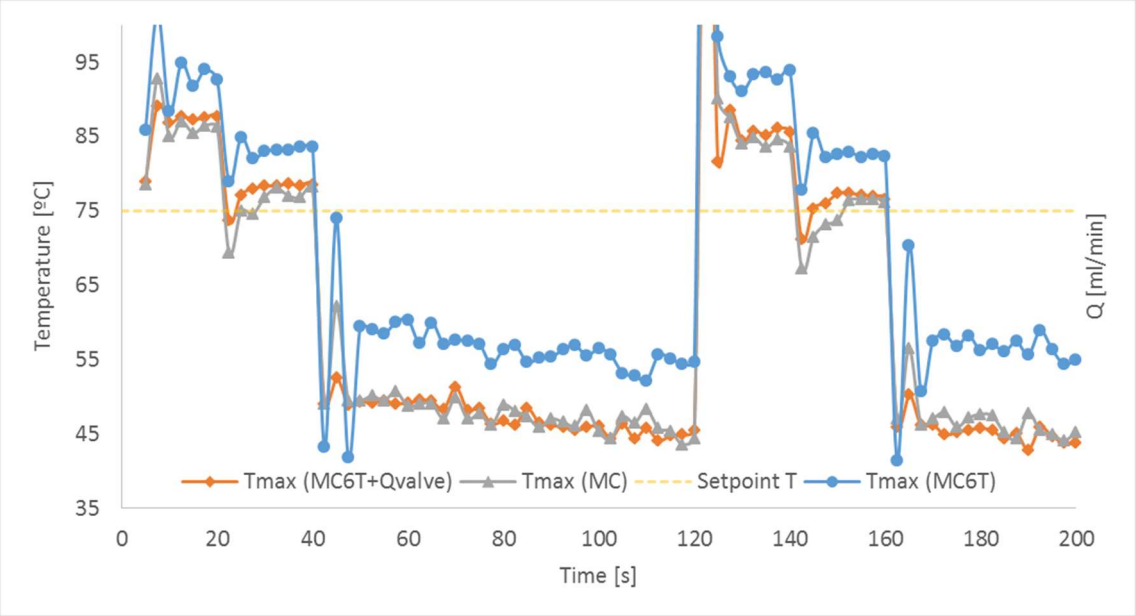

Figure 31. Maximum temperature of the three compared devices along time for variable flow rate.

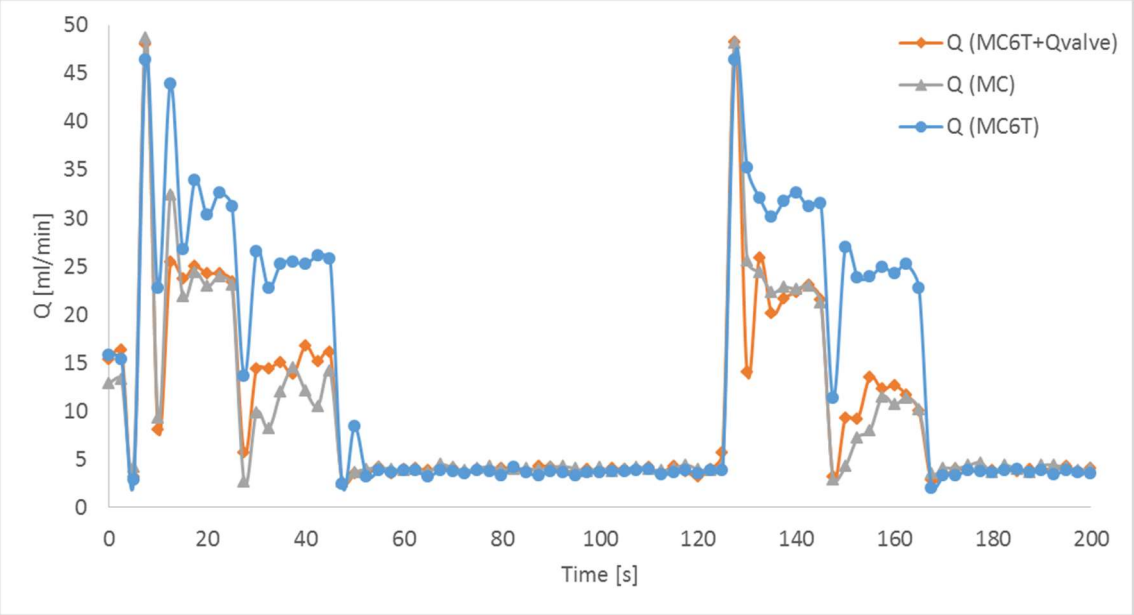

Figure 32. Flow rate variation along time for the three assessed devices.

Pressure drop

However, the intrinsic low pressure drops of the STREAMS geometry (array of microfluidic cells) allow the reduction of the main drawback of microchannels: the pressure drop (Figure 33). In the case of the STREAMS solution including Self Adaptive valves, the pressure drop is lower than in MC when the heat extraction capacity needs to be high (high heat load). This result is obtained even if, as observed with fixed coolant flow rate, the valves induces high pressure drops in the circuit.

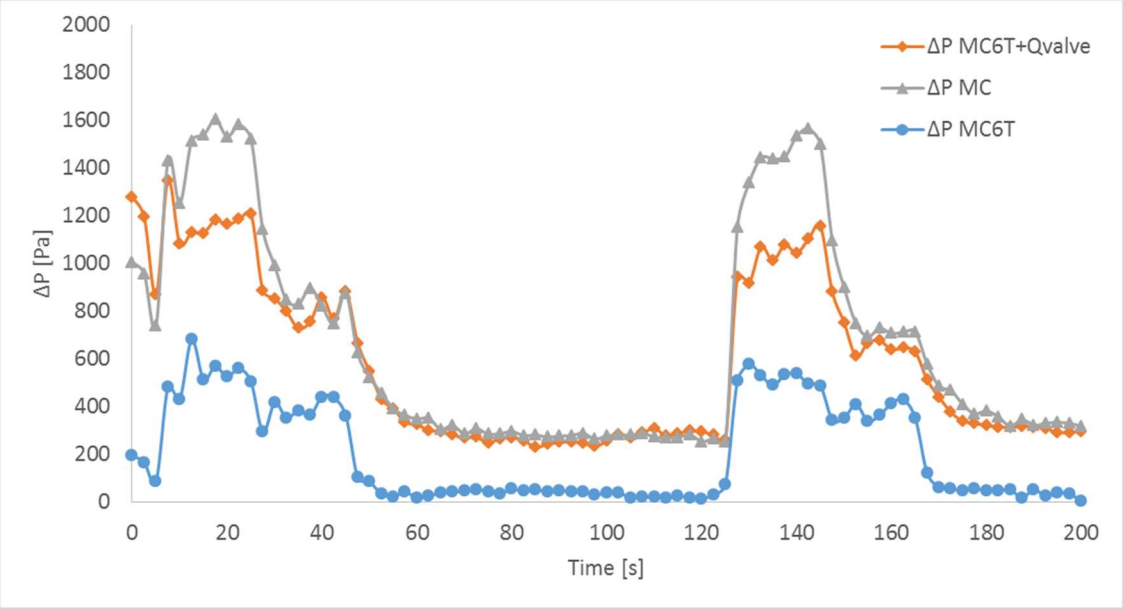

Figure 33. Pressure drop of the three devices along time for variable flow rate.

Pumping Power

These behaviors imply that both STREAMS cooling solutions (with and without self-Adaptive Valves) enhance the pumping power savings with respect to conventional microchannels, with and without tailored flow rates (Figure 34).

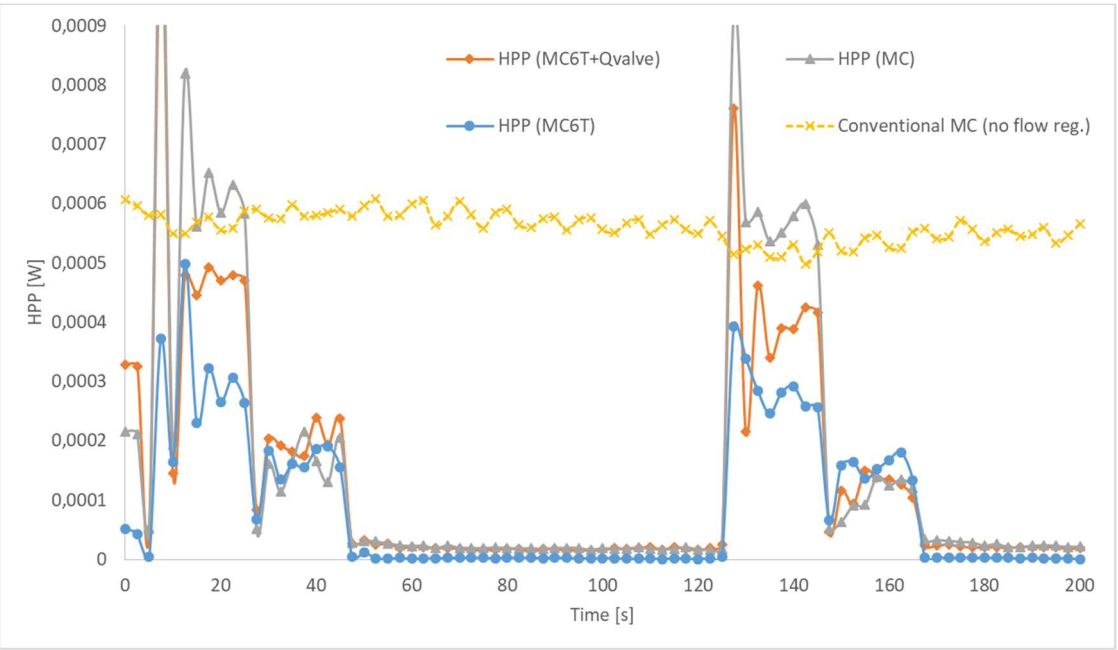

Figure 34. Temperature distribution in MC for several flow rates.

Along the time period considered, the savings of pumping energy of the STREAMS cooling device, with and without Self-Adaptive valves, with respect to microchannels, are 15,5% and 45,6%, respectively (Table 12). This comparison is made with an equal flow rate control algorithm and so, it depends only on the geometries of the cooling solutions.

When the STREAMS cooling solution are compared to conventional microchannels without tailored flow rates (state of the art), the hydraulic pumping power savings become of 74,7% and 83,7%, for the array of microfluidic cells with and without Self-Adaptive valves, respectively.

Table 12. Summary of WP2 Microfluidic PoC results.

Flow rate	Geometry	Q_{av}	ΔP_{av}	Hydraulic Pumping Power			HPP/Pxip	ΔTmax
				Energy (time integration)	Savings/ [MC + flow control]	Savings/ [Conv. MC]		
		ml/min	Pa	J	%	%	%	ºC
Tailored flow rate	MC6T	13,8	209	1,85E-02	45,6	83,7	7,88E-03	43,6
	MC6T + valve	9,9	589	2,87E-02	15,5	74,7	1,29E-02	33,4
	MC	9,6	680	3,40E-02			1,30E-02	43,9
Fixed flow rate	MC	22,1	1526	1,14E-01			1,71E-01	48,9

Temperature non-uniformity

Apart from the pumping power reduction, STREAMS cooling solution aimed to reduce the temperature non-uniformities of the chip. We can observe in Figure 35 and Table 12 (values at t=130s) that the actuation of the Self-Adaptive valves generates a reduction of this parameter by about 10ºC with respect to conventional microchannels, and even up to 15ºC without flow control.

MC6T+Qvalve

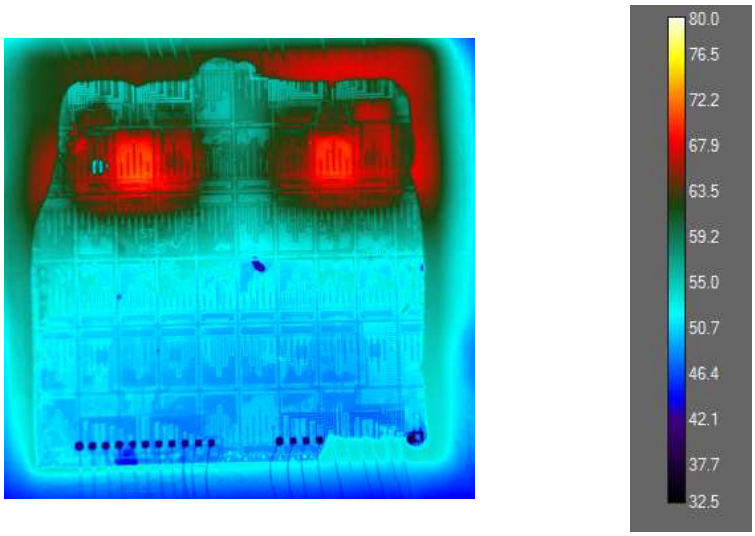

MC – fixed Q

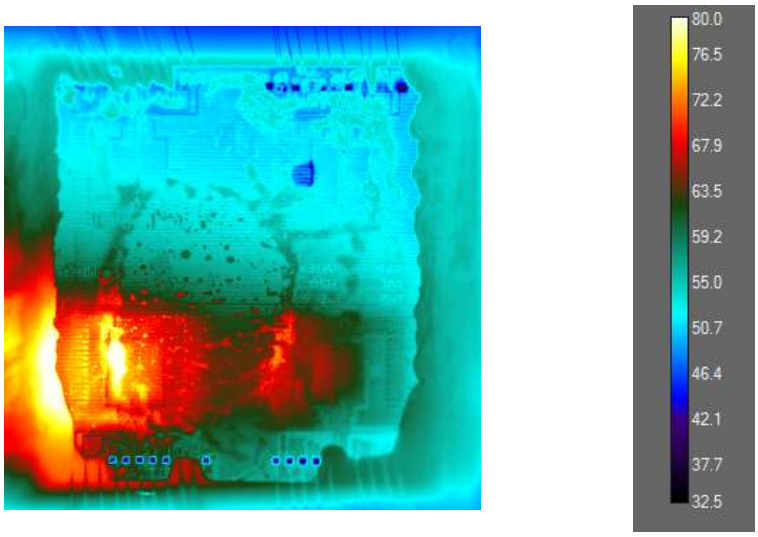

MC6T

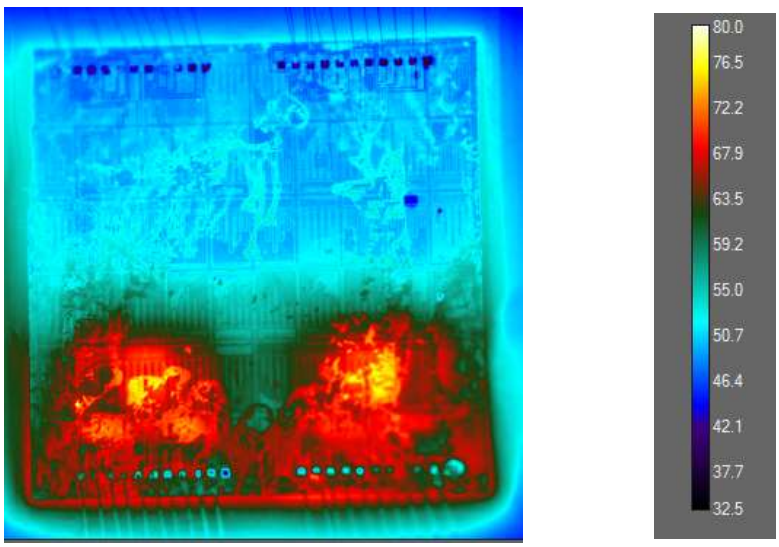

Figure 35. Temperature distribution for the maximum heat load (t=130s).

3.3. Reliability assessment

The reliability assessment has been limited to:

- the observation of destructed samples (Figure 36)

- the cycling of the self-adaptive valve aperture, observed in the attached video and in Figure 26. The applied boundary conditions have been maintained until achieving 1000 cycles without observing (qualitatively) variations of the valve behavior.

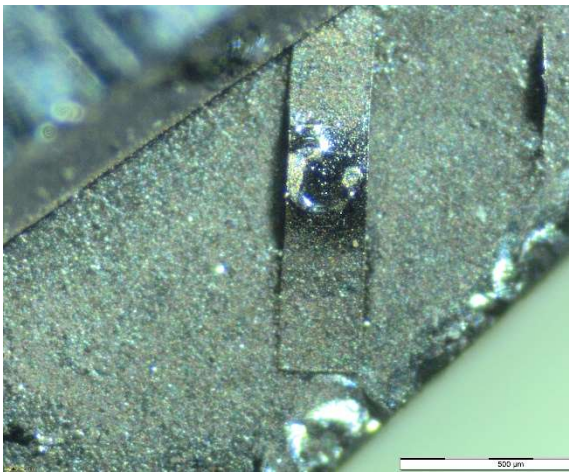

a) Device submitted to high temperature: some plastic deformations on fins

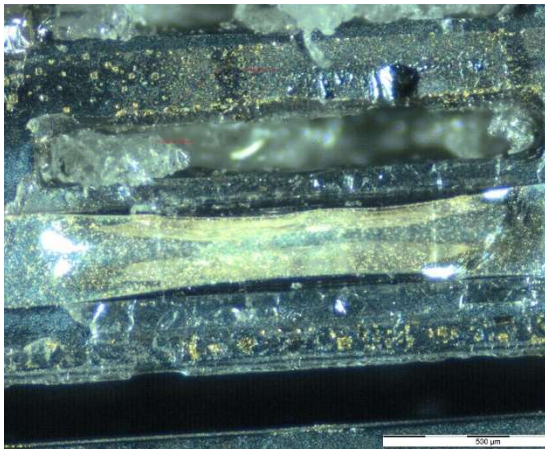

b) Valves: Lateral deformation

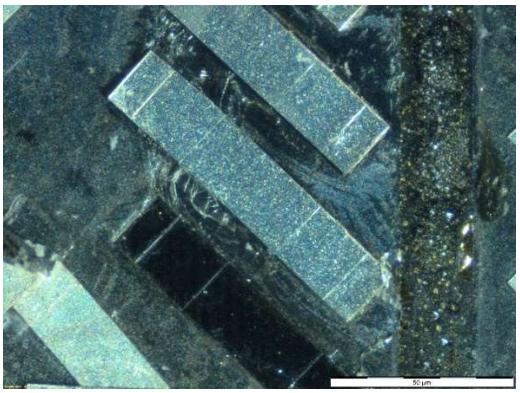

c) Fin removed

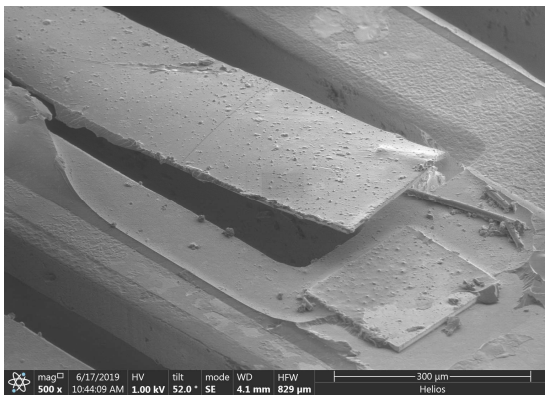

d) Broken valves

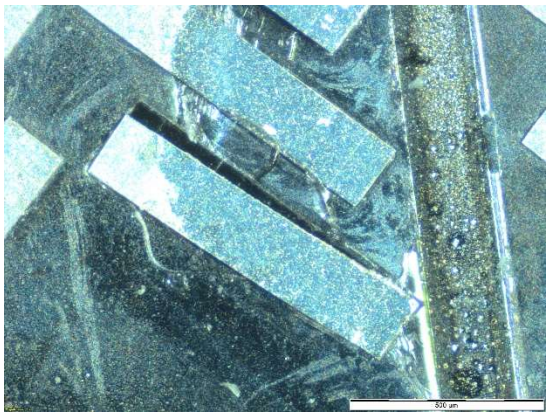

e) Anchor broken

Figure 36. Reliability of the samples. Microscopy and SEM pictures

4. CONCLUSIONS AND FUTURE WORK

In this report, the proposed self-adaptive fins and valves have been experimentally demonstrated.

In a first stage, the capacity of the Self-Adaptive fins to locally boost the heat transfer, demonstrated numerically, has been experimentally validated.

In a second stage, a series of tests have been carried out at fixed flow rate to characterize the cell array cooling solutions with and without microvalves. The result demonstrated that the STREAMS cooling scheme allows to reduce drastically one of the major drawback of microchannel cooling devices: the pressure drops.

As a consequence of the geometry of the STREAMS cooling solution, the total thermal resistance of the microchannel cooling device is lower (but in the same order of magnitude) than for the array of microfluidic cells. However, this result was expected and does not affect the thermo-hydraulic performance of the device, as the tailored flow rate and self-adaptive distribution of the coolant across the array of microfluidic cells compensate this characteristic.

For the array of microfluidic cells with self-adaptive valves (MC6T+Valve), the temperature distribution pattern corresponds to the geometry of the microfluidic cells. This result confirms the capacity of the STREAMS cooling solution to tailor the distribution of the heat extraction capacity for non-uniform heat loads.

For a given set of fixed boundary conditions (Inlet temperature; Flow rate; Heat flux), the opening and closing of the self-adaptive valves, leading to a passive control of the distribution of the heat extraction capacity, has been observed and validated.

Finally, a time dependent and non-uniform heat load scenario has been applied. The analysis of these results demonstrated that all the objectives defined for the STREAMS cooling solution have been reached (Table 13).

Also, the achievement of the STREAMS objectives, as defined at M6, are clearly demonstrated in Figure 37.

Table 13. STREAMS objectives vs State of the Art for the cooling functionality and WP2 PoC Demonstrator.

Devices characteristics		**STREAMS objective**	**STREAMS Numerical assessment**	**SoA 1** Conventional Microchannels (*)	**SoA 2** IBM [1]	**WP2 PoC Demo**
Cooling technology		Self adaptive cooling device	Self adaptive cooling device *or* tailored Microchannel cooling device	Microchannels	Advanced Microchannels	**Self adaptive cooling device**
Pressure drop		25% reduction	Max 0,03 bar	-	0,3 bar	**38,6% reduction**(1)
Thermal Resistance		Equal	$1{,}7.10^{-5}$ Km^2/W	-	2.10^{-5} Km^2/W	**Locally equal** (2)
Hydraulic Pumping Power (HPP)	**Absolute**	50% reduction	5% of Microchannel HPP	8 mW	-	**74,7% reduction**
	Relative	HPP/P_{chip}< 0,05 %	HPP/P_{chip}= 0,02 %	-	HPP/P_{chip} = 0,17 %	**HPP/P_{chip} = 0,0129 %**

(1) With respect to conventional microchannels. (Average value)

(2) Through the tailored distribution of the coolant

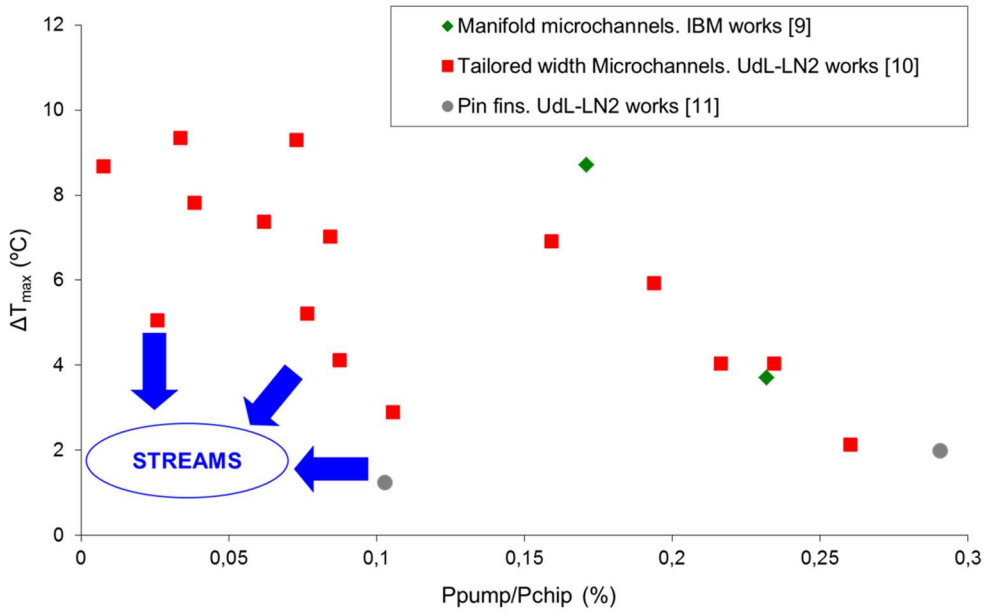

a) STREAMS objective – from proposal

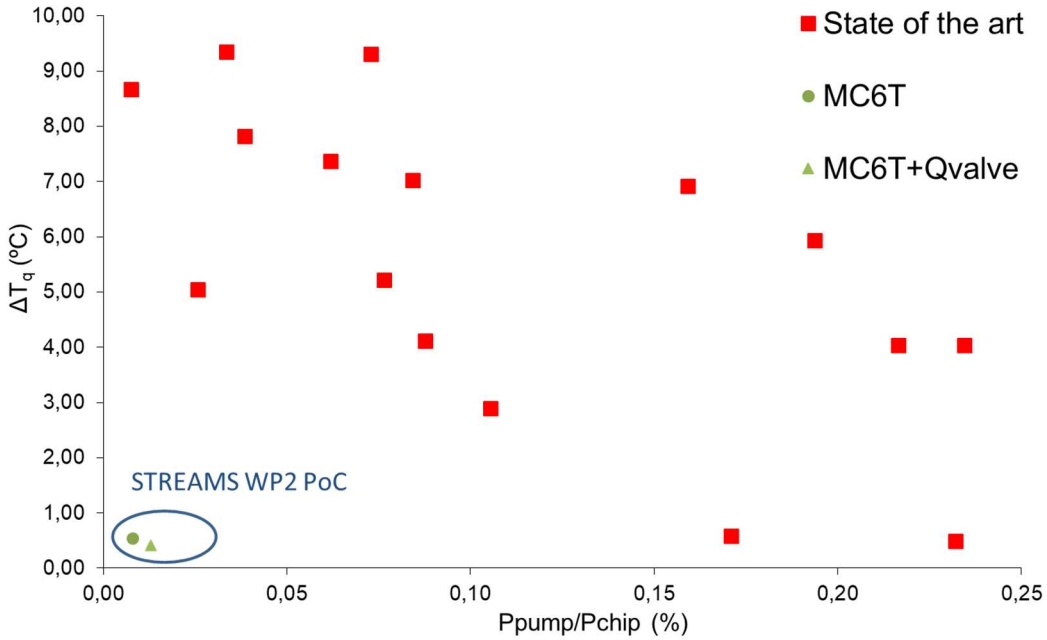

b) STREAMS achievements – beyond proposal

Figure 37. Performance of STREAMS cooling solution a) Objectives defined at M6 General Assembly, b) Proof of Concept.

ONGOING WORKS & Publications

The achievement of the STREAMS objectives of the cooling solution proposed has been demonstrated. However, new batches are in fabrication phase in order to:

- Achieve a broader range of device configurations. This planning was generated to verify the performance of the STREAMS cooling solution (achieved), but also to provide material for future publications.
- Extend the reliability tests. Indeed, this work needs further efforts and results in order to advance in the TRLs of the technology, now that the concept has been experimentally validated.